Rational exploration of 2,4-diaminopyrimidines as DHFR inhibitors active against *Mycobacterium abscessus* and *Mycobacterium avium*, two emerging human pathogens

Matheus A. Meirelles,[1,#] Vitor M. Almeida,[2,#] Jaryd R. Sullivan,[3,4,5] Ian de Toledo,[1] Caio Vinicius dos Reis,[2] Micael R. Cunha,[2] Rachael Zigweid,[6,7] Abraham Shim,[6,7] Banumathi Sankaran,[8] Elijah L. Woodward,[7,9] Steve Seibold,[7,9] Lijun Liu,[7,9] Mohammad R. Mian,[7,9] Kevin P. Battaile,[10] Jennifer Riley,[11] Christina Duncan,[11] Frederick R. C. Simeons,[11] Liam Ferguson,[11] Kevin D. Read,[11] Scott Lovell,[7,9] Bart L. Staker,[6,7] Marcel A. Behr,[3,4,5,12] Ronaldo A. Pilli,[1,*] Rafael M. Couñago[2,13,*]

1 - Department of Organic Chemistry, Institute of Chemistry, University of Campinas, UNICAMP, 13083-970-Campinas, SP, Brazil.
2 - Center of Medicinal Chemistry (CQMED), Center for Molecular Biology and Genetic Engineering (CBMEG), University of Campinas, UNICAMP, 13083-886-Campinas, SP, Brazil.
3 - Department of Microbiology & Immunology, McGill University, Montréal H3A 2B4, Canada.
4 - Infectious Diseases and Immunity in Global Health Program, Research Institute of the McGill University Health Centre, Montréal H4A 3J1, Canada.
5 - McGill International TB Centre, Montréal H4A 3S5, Canada.
6 - Center for Infectious Disease Research, Seattle Children's Research Institute Seattle Washington 98109 USA
7 - Seattle Structural Genomics Center for Infectious Disease (SSGCID), Seattle, Washington, 98109, USA
8 - Molecular Biophysics and Integrated Bioimaging, Berkeley Center for Structural Biology, Lawrence Berkeley National Laboratory, Berkeley, CA, USA.
9 - Protein Structure and X-ray Crystallography Laboratory, Del Shankel Structural Biology Center, University of Kansas, Lawrence, Kansas 66047, USA.
10 - New York Structural Biology Center, Upton, New York 11973, USA.
11 - Drug Discovery Unit, Wellcome Centre for Anti-Infectives Research, Division of Biological Chemistry, University of Dundee, Dundee DD1 5EH, UK.
12 - Department of Medicine, McGill University Health Centre, Montréal H4A 3J1, Canada.
13 - Structural Genomics Consortium and Division of Chemical Biology and Medicinal Chemistry, UNC Eshelman School of Pharmacy, University of North Carolina, Chapel Hill, North Carolina 27599, USA

# These authors contributed equally to this work.
* Corresponding authors: rafael.counago@unc.edu; rapilli@unicamp.br

Abstract

Nontuberculous mycobacteria (NTM) are emerging human pathogens linked to severe pulmonary diseases. Current treatments involve the prolonged use of multiple drugs and are often ineffective. Bacterial dihydrofolate reductase (DHFR) is a key enzyme targeted by antibiotics in Gram-negative bacterial infections. However, existing DHFR inhibitors designed for Gram-negative bacteria often fail against mycobacterial DHFRs. Here, we detail the rational design of NTM DHFR inhibitors based on **P218**, a malarial DHFR inhibitor. We identified **8**, a 2,4-diaminopyrimidine exhibiting improved pharmacological properties and activity against purified DHFR and whole cell cultures of two predominant NTM species: *Mycobacterium avium* and *Mycobacterium abscessus*. This study underscores the potential of **8** as a promising candidate for the *in vivo* validation of DHFR as an effective treatment against NTM infections.

Introduction.

Nontuberculous mycobacteria (NTM) are opportunistic human pathogens mainly responsible for pulmonary disease (NTM-PD), particularly in individuals with structural airway diseases like cystic fibrosis, chronic obstructive pulmonary disease, or silicosis.[1] They can also cause lymphadenitis, skin and soft tissue infections, cardiac infections, bone and joint infections, and disseminated diseases.[2] Despite substantial prevalence in countries like the USA, Portugal, Italy, England, China, and Brazil, NTM infections remain underestimated since they have not been recognized as a public health concern.[3–10]

Classically, NTMs are categorized into rapid and slow growers based on their growth rates on solid media. Rapid growers develop mature colonies within seven days, while slow growers take longer. Notable rapid growers that cause human disease include the *Mycobacterium abscessus* complex (comprising *M. abscessus subsp. abscessus*, *M. abscessus* subsp. *bolletii*, and *M. abscessus* subsp. *massiliense*), *M. fortuitum*, and *M. chelonae*. Slow growers causing human disease include the *Mycobacterium avium* complex (comprising *M. avium*, *M. intracellulare*, and *M. chimaera*), *M. kansasii*, and *M. xenopi*. Most NTM-PD are caused by the *M. avium* complex, *M. abscessus* complex and *M. kansasii*.[11,12]

Currently, the primary treatment for most NTM infections involves macrolide-based antibiotics, such as clarithromycin or azithromycin. Treatment protocols for infections caused by slow-growing NTMs also incorporate ethambutol and rifampicin, whereas protocols for fast-growing NTMs include an aminoglycoside along with cefoxitin, imipenem, or tigecycline.[13,14] These therapeutic approaches may extend up to 18 months and frequently result in drug-induced toxicities and side effects.[15–17] Cure rates vary significantly, with *M. malmoense* infections achieving 80–90 % success, but only 30–50 % success for *M. abscessus* infections.[18] Consequently, the development of novel and more effective treatments for NTMs remains a critical research focus. However, a significant challenge is the inherent low susceptibility of NTM to most antibiotics, including those used to treat tuberculosis.[16,19]

Dihydrofolate reductase (DHFR) is an essential enzyme in folate metabolism, catalyzing the reduction of dihydrofolate to tetrahydrofolate during the synthesis of deoxythymidine monophosphate, a crucial precursor in DNA synthesis.[20] Due to its indispensable role in cell metabolism, DHFR is highly conserved across various organisms. Consequently, it has become a recognized target for treating diverse diseases, including bacterial and fungal infections, as well as human chronic diseases such as cancer (**Figure 1**). Trimethoprim (TMP), a 2,4-diaminopyrimidine, has been the most successful inhibitor of bacterial DHFRs. Since the 1960s, TMP has been effectively used in clinical settings to treat a broad spectrum of bacteria causing urinary tract infections.[21]

Although the use of DHFR inhibitors to treat mycobacterial infections has not been validated in the clinic, there is mounting evidence that DHFR is a vulnerable target in these bacteria. For example, disrupting the folate pathway in *M. tuberculosis* with DHFR inhibitors leads to cell death and it has been shown that the anti-TB drug *p*-aminosalicylic acid (PAS) is a pro-drug that targets *M. tuberculosis* DHFR.[22–24] Additionally, DHFR inhibitors have been shown to inhibit the growth of *M. avium* and *M. abscessus* in cultures, underscoring the potential of this chemical class as anti-infective agents against nontuberculous mycobacterial (NTM) infections.[25–31] Consequently, efforts have been made to develop novel anti-folate compounds targeting Mycobacterial DHFRs.[32]
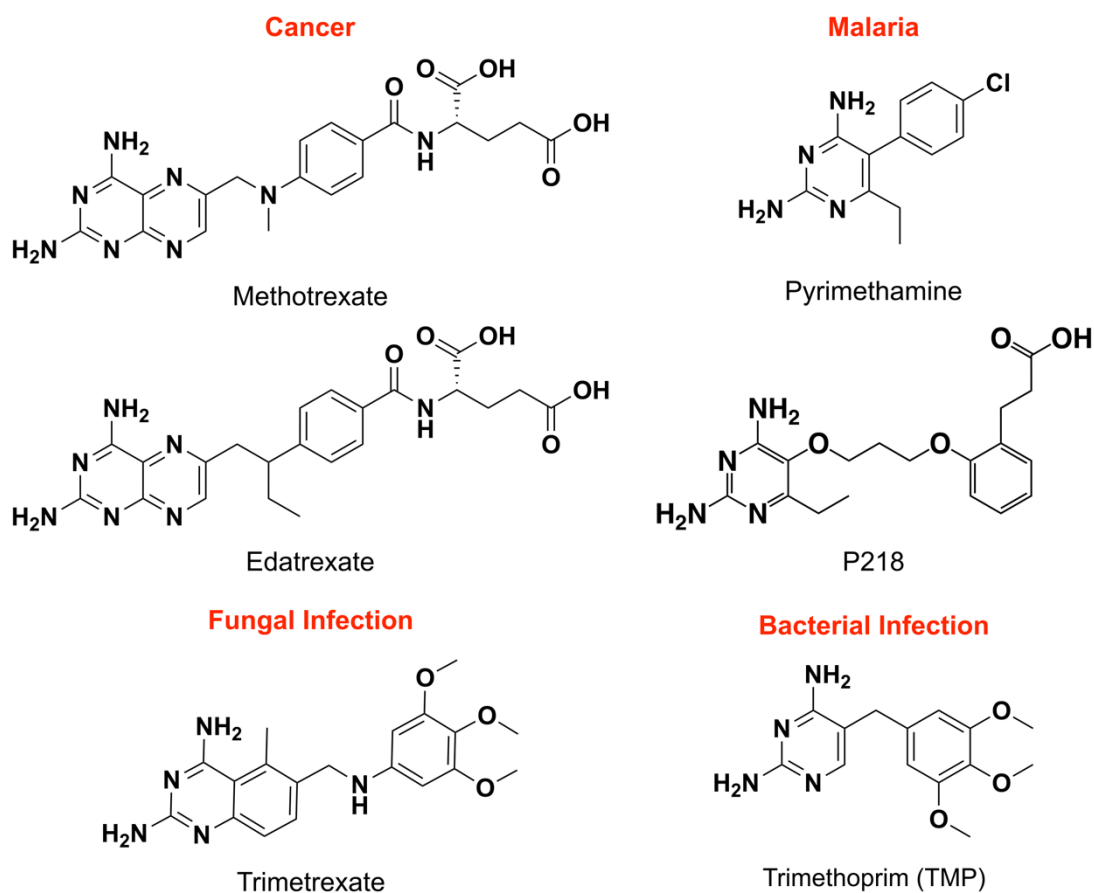
4

FIGURE 1

Figure 1 – Examples of DHFR inhibitors and their clinical applications (in red).

P218 is a 2,4-diaminopyrimidine compound initially developed for malaria treatment, which has also demonstrated potent activity against mycobacterial DHFRs, sparking interest in its application against these pathogens.[33,34] Recent clinical studies showed that **P218** can safely protect human patients against malaria.[35] Additionally, clinical isolates of *Plasmodium* resistant to other antifolates, such as pyrimethamine, due to mutations in the DHFR enzyme are still sensitive to **P218**.[33,36,37] Biochemical and structural studies suggest that the emergence of *Plasmodium* resistance to **P218** may be slowed down by the compound's tight binding and long on-target residence time, as it interacts with the enzyme in a similar way to the enzyme's dihydrofolate substrate.[33]

In this study, we detail the rational design of **P218** analogues with potent activity against DHFR enzymes from two predominant NTM species: *M. avium* and *M. abscessus*. Some of our DHFR inhibitors exhibited greater potency in inhibiting the growth of these NTM species in culture than the parent compound, **P218**, and amikacin, an aminoglycoside antibiotic that targets bacterial protein synthesis and is currently employed to treat NTM infections. Additionally, both *in vitro* and *in vivo* profiling of our most active compounds revealed enhanced pharmacological properties compared to the parent molecule, **P218**. Future development efforts for this compound series will focus on optimizing bioavailability and reducing plasma protein binding.

Results and Discussion

P218 is a potent, whole cell-active inhibitor of NTM DHFRs

Previous work has established **P218** as a potent inhibitor of mycobacterial DHFRs, including those from *Mycobacterium tuberculosis* and *Mycobacterium ulcerans*.[34] To evaluate its efficacy against the NTM enzymes from *Mycobacterium avium* (Mav) and *Mycobacterium abscessus* (Mab), we employed a well-established biochemical assay.[34] This assay utilizes NADPH fluorescence to estimate **P218**'s inhibitory constant (K_i) towards these enzymes. Our findings revealed that **P218** is a potent inhibitor of DHFR in both NTM species (**Figure 2A**). This outcome was

6

anticipated due to the amino acid sequence and structural similarities among mycobacterial DHFRs (**Figure 3** and see below).

More importantly, further studies revealed that **P218** inhibited the growth of *M. abscessus* and *M. avium*, with minimal inhibitory concentrations (MICs) of 28.0 and 0.3 µM, respectively (**Figure 2B**). The notable difference in potency between the two bacteria may be attributed to variations in compound permeability and metabolism.[38,39] Despite these differences, our data collectively indicate that **P218** is effective against both NTM species, highlighting its potential as a therapeutic agent.
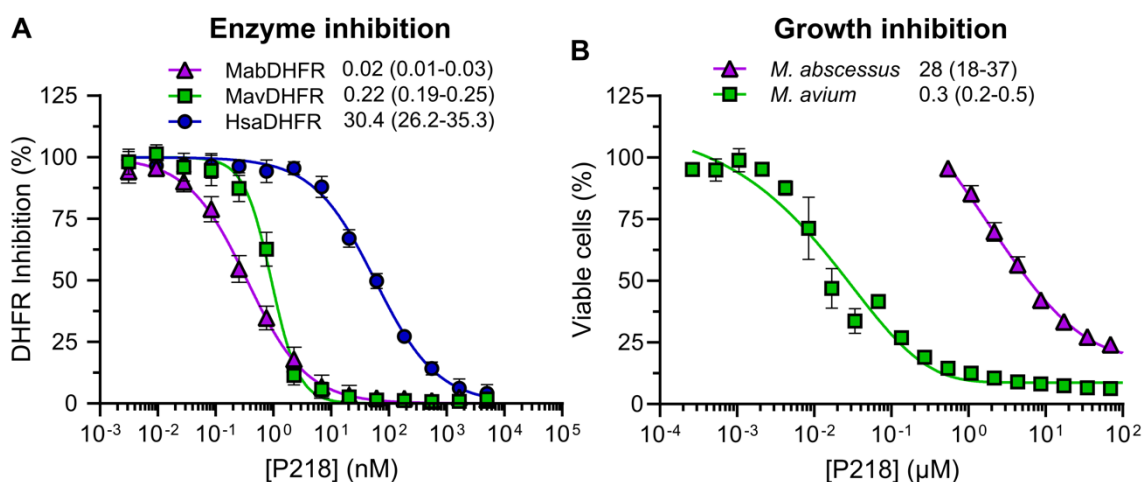
FIGURE 2

Figure 2 – **P218** is a potent, bioactive inhibitor of *M. avium* and *M. abscessus* DHFR enzymes. **A** Dose-response curves for **P218** and the DHFR enzymes from *M. avium* (MavDHFR), *M. abscessus* (MabDHFR) and humans (HsaDHFR). Data shown are mean ± SEM of at least six independent experiments performed in duplicates. Indicated K_i values were obtained by applying the Cheng-Prusoff equation to IC_{50} values estimated following the fitting of the experimental data to the four-parameter sigmoidal dose-response equation. **B** Determination of **P218** minimum inhibitory concentration (MIC in µg/mL) for *M. avium* and *M. abscessus*. MIC values indicated were calculated by extrapolating a tangent from the inflexion point of a fitted Gompertz curve (colored solid lines) to the no-growth line.[40] In **A** and **B**, numbers in parenthesis are CI 95 %.

Structure of MabDHFR complexed with NADP and **P218**

To better understand **P218** binding mode to mycobacterial DHFR and inform compound development, we obtained the co-crystal structure of MabDHFR complexed with both the inhibitor **P218** and co-factor NADP at 2.0 Å resolution (**Additional Data File 1 and Figure 3A;** PDB ID 7K6C). This structure revealed a central β-sheet (β1-β11) encased by four α-helices (α1-α4), showcasing a high degree of structural similarity (root mean square deviation of equivalent Cα atoms < 1.0 Å) with existing mycobacterial DHFR structures, including those from *M. tuberculosis* (PDB ID: 5U26) and *M. ulcerans* (PDB ID: 6UWW) complexed with NADP and **P218**, as well as *M. avium* complexed with NADP and a distinct 2,4-diaminopyrimidine (DAP)-based inhibitor (PDB ID: 2W3W).
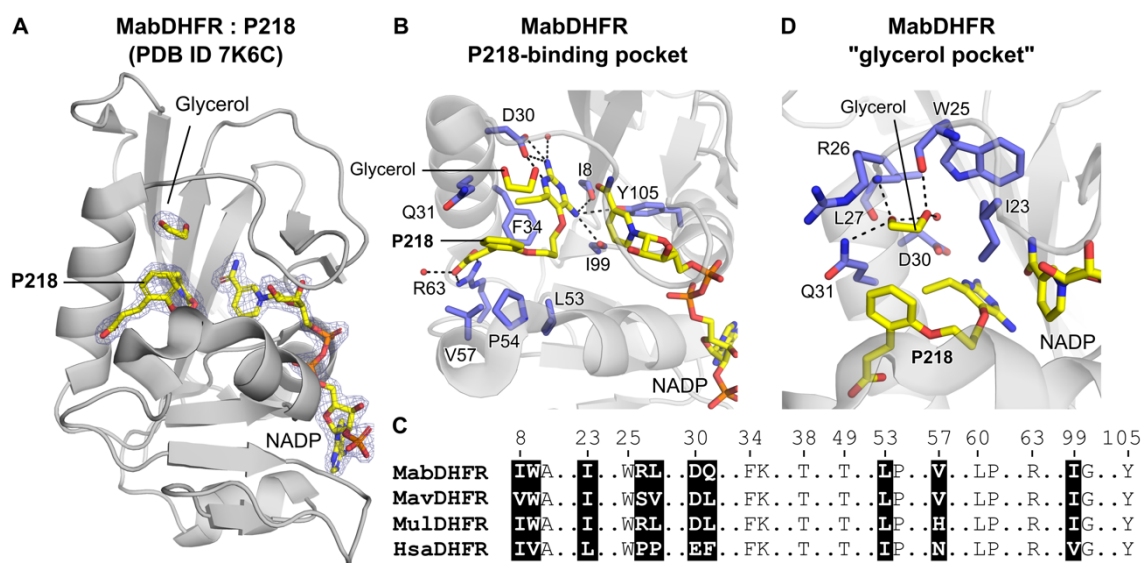
FIGURE 3

Figure 3 – Structure of MabDHFR in complex with **P218** and comparison of ligand and glycerol binding sites of mycobacterial and human DHFRs. **A** Overall structure of MabDHFR (cartoon) bound to inhibitor **P218** and co-factor NADP. Electron density map (omit map contoured at 1.5 σ - gray mesh) is shown for glycerol, **P218** and NADP (sticks). **B,D** Details of MabDHFR **P218**- (**B**) and glycerol- (**D**) binding pockets. Black dashed lines depict potential hydrogen bonds. **C** Structure-based sequence alignment of equivalent *M. abscessus* (Mab), *M. avium* (Mav), *M. ulcerans* (Mul) and human (Hsa) DHFR residues within a 5 Å radius of **P218** and glycerol bound to MabDHFR. Black boxes highlight non-identical residue.

The electron density map for **P218**, NADP, and the surrounding protein residues at the active site of MabDHFR was of excellent quality, allowing us to model both the inhibitor and the cofactor unambiguously (**Figure 3A**). The DAP moiety of the inhibitor anchored **P218** deep within the enzyme's active site, forming hydrogen bonds with the side chain atoms of Asp30 and Tyr105, as well as the main chain atoms of Ile8 and Ile99 (**Figure 3B**). Additionally, the DAP moiety of **P218** was sandwiched between the aromatic ring of a structurally conserved phenylalanine residue (Phe34 in MabDHFR) and the amide group of the cofactor NADP. The residues interacting with DAP in the MabDHFR structure are conserved across various DHFRs (**Figure 3C**), with similar interactions observed in the co-crystal structures of human, *M. tuberculosis*, and *M. ulcerans* enzymes bound to **P218**. The central 5-atom ether moiety of **P218** did not directly interact with any protein atoms. Nevertheless, this flexible moiety enabled the ligand to maneuver around the side chain of the structurally conserved Phe residue (Phe34 in MabDHFR), positioning **P218**'s benzyl group within a hydrophobic patch formed by the side chains of residues Leu53, Pro54, and Val57. Moreover, the α-carboxylate group of the ligand engaged in a bidentate hydrogen bond with a conserved Arg residue (Arg63 in MabDHFR), further stabilizing the interaction.

Previous structural analyses have uncovered a unique "glycerol pocket" within the active site of *M. tuberculosis* DHFR. [41] This distinctive feature is also consistently present across mycobacterial DHFR structures, including those from *M. avium*, *M. ulcerans*, and the *M. abscessus* DHFR detailed in our study (**Figure 3D**). In our MabDHFR structure, a glycerol molecule, presumably derived from the crystallization cocktail, was found within this pocket, delimited by residues Ile23, Trp25, Arg26, Leu27, Asp30, and Gln31. This glycerol molecule established polar interactions with the main chain atoms of Trp25 and Leu27, the side chain nitrogen of Gln31, and a water molecule from the solvent, and was positioned within 5 Å of the ethyl group of **P218**. The overall high sequence and structural conservation observed among mycobacterial DHFRs also extends to the **P218** binding site. Amino acids within a 5 Å radius of the inhibitor were highly conserved across DHFRs from *M. tuberculosis*, *M. ulcerans*, *M. avium*, and *M. abscessus*, with 17 out of 20 amino acids being identical (**Figure 3C**).

While the structural and sequence conservation among mycobacterial DHFRs provides a solid foundation for targeted inhibitor design, the differences between these enzymes and the human (Hsa)DHFR offer opportunities to rationally develop selective compounds that inhibit mycobacterial enzymes without affecting the human protein. First, the human DHFR's substrate binding pocket diverges significantly from its mycobacterial counterparts, with only 13 out of the 20 residues within a 5 Å radius of **P218** shared between them. One effect of this variation is steric hindrances from the side chain of Phe31 in the human DHFR (replaced by Leu30/Leu32/Gln31 in Mul-, Mav-, and MabDHFR, respectively), which block **P218**'s carboxylate group from forming hydrogen bonds with the conserved arginine residue (Arg63 in MabDHFR), drastically reducing **P218**'s efficacy against the human enzyme by at least 140-fold compared to mycobacterial enzymes (**Figure 2A**). Additionally, the glycerol pocket found in mycobacterial DHFRs is absent in the human enzyme, where the equivalent space is occupied by hydrophobic side chains from residues Leu22, Pro26, and Phe31 (**Figure 3C**).

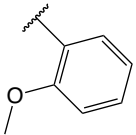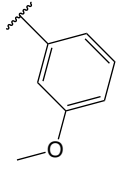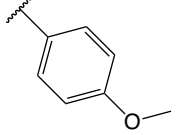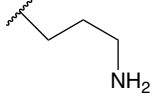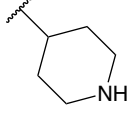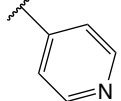## Structure-activity relationship (SAR) of novel P218 derivatives.

The structural analyses above indicated an opportunity to explore the glycerol pocket found in mycobacterial DHFRs and rationally design novel **P218** derivatives having improved activity towards the *M. abscessus* and *M. avium* enzymes, while sparing the human enzyme. Although challenging, reduced activity towards the human enzyme is particularly desirable. Loss of human DHFR function is detrimental to various human-derived cell types and treatment of human patients with potent inhibitors of human (*Hsa*)DHFR, such as methotrexate, is known to cause toxic effects, most likely due to a reduction of folic acid in the body.[42,43]

To increase compound selectivity towards the mycobacterial enzymes, we focused on replacing the ethyl group in **P218** with different substituents to better complement the glycerol pocket found in the NTM enzymes (**Table 1**). We assessed these novel **P218** analogues using the above-described enzymatic assay and in-house purified *M. abscessus*, *M. avium*, and human DHFR enzymes. Despite the challenges in co-crystallizing NTM enzymes with **P218** analogues, we successfully obtained high-resolution co-crystal structures of *M. ulcerans* (Mul)DHFR in

complex with NADP and selected inhibitors (**Additional Data File 1**). These MulDHFR co-structures served as valuable surrogates for understanding compound interactions with NTM and human enzymes, thereby informing our structure-activity relationship (SAR) analysis. These structural analyses were facilitated by the high amino acid identity level found for residues within the glycerol pocket of different DHFR enzymes (**Figures 3C,D**). Notable exceptions are a single amino acid substitution from Leu30 in MulDHFR to Gln31 in MabDHFR and two substitutions from Arg25 and Leu26 in MulDHFR to Ser27 and Val28 in MavDHFR.

TABLE 1

Table 1 – Inhibitor constant (pK_i) for P218 analogues against mycobacterial and human DHFRs

Compound	R	MavDHFR[a]	MabDHFR[a]	HsaDHFR[a]
P218		0.22 (0.19-0.25)	0.02 (0.01-0.03)	30.4 (26.2-35.3)
1	H	11.3 (9.78-12.5)	23.9 (20.6-27.7)	> 1,250
2		0.20 (0.12-0.26)	0.02 (0.01-0.04)	7.15 (5.12-10.0)
3		0.23 (0.18-0.27)	0.20 (0.17-0.23)	108 (85-136)
4	OH	0.25 (0.21-0.28)	0.12 (0.10-0.14)	114 (96-137)
5		> 1,250	> 1,250	> 1,250
6		> 1,250	> 1,250	> 1,250
7		> 1,250	> 1,250	> 1,250
8		0.32 (0.28-0.37)	0.03 (0.02-0.03)	> 1,250
9		0.36 (0.30-0.40)	0.41 (0.37-0.47)	521 (451-600)
10	F_3C	1.44 (0.98-1.80)	1.02 (0.75-1.38)	> 1,250
11	F_3C	97.8 (85.1-108.0)	7.76 (5.99-10.01)	> 1,250
12	CF_3	3.41 (2.46-4.00)	10.6 (8.4-13.2)	> 1,250

13		10.8 (7.8-13.7)	5.17 (4.26-6.26)	> 1,250
14		3.06 (2.11-3.94)	0.31 (0.26-0.36)	17.2 (13.7-21.3)
15		0.27 (0.22-0.30)	0.42 (0.34-0.50)	175 (130-237)
16		12.2 (11.1-13.2)	8.96 (8.79-9.15)	> 1,250
17		3.22 (2.83-3.56)	9.14 (9.05-9.23)	> 1,250
18		0.88 (0.77-0.97)	1.85 (1.37-2.47)	> 1,250

[a] inhibition constant (K_i) values calculated using the Cheng-Prusoff equation from IC_{50} values determined from at least two independent experiments performed in duplicates. Values in parenthesis are CI 95 %. Dose-response curves used for K_i calculation can be found in Supplementary Figure S1.

Before investigating the use of bulkier groups in place of **P218**'s ethyl group, we first replaced this moiety with a hydrogen atom, yielding compound **1**. This modification greatly reduced activity for the two mycobacterial enzymes (> 50-fold) and rendered the compound virtually inactive (K_i > 1250 nM) towards the human enzyme. Most residues within the DHFR glycerol pocket have hydrophobic side chains. Thus, removal of **P218** ethyl group may disrupt hydrophobic interactions between this region of the inhibitor and the side chains of surrounding protein amino acids. These observations underscored the relevance of **P218** ethyl group for both compound potency and selectivity.

We next investigated the impact of extending the ethyl aliphatic chain in **P218**. Compound **2** with a *n*-propyl was equipotent towards the two NTM enzymes and ~4-fold more potent towards the human DHFR than **P218**. Extending the aliphatic chain to an *n*-pentyl in **3** had no effect on compound potency towards the *M. avium* enzyme but resulted in a 10-fold potency drop for the *M. abscessus* DHFR and 3.5-fold reduction in potency for the human enzyme compared to **P218**. The co-crystal structure of MulDHFR in complex with NADP and **3** showed the inhibitor's *n*-pentyl moiety sandwiched between the hydrophobic side chains of Ile22 and Leu30 **(Figure 4A)**. In the human and *M. abscessus* enzymes, MulDHFR Leu30 is replaced by amino acids with bulkier side chains (Gln31 and Phe31 in Mab- and HsaDHFRs, respectively). Steric clashes between the compound *n*-pentyl moiety and the bulkier side chain of these amino acids may explain **3** reduced activity towards these enzymes.

FIGURE 4
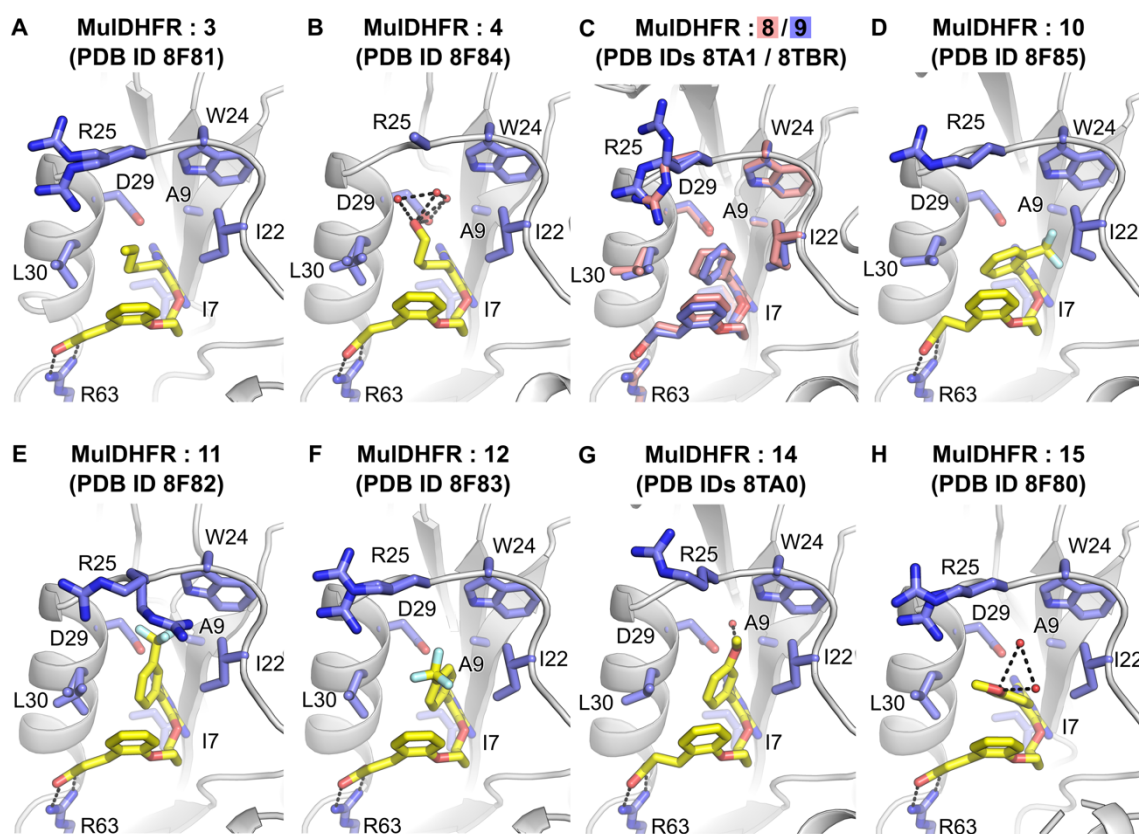
Figure 4 – Binding mode details of various **P218** analogues co-crystallized with MulDHFR. **A-H** Protein residues relevant for inhibitor or glycerol binding are shown as sticks; water molecules are shown as red spheres and potential hydrogen bonds are shown as black dashed lines. Panel **C** depicts the superimposed structures of MulDHFR bound to **8** (carbon atoms for highlighted protein residues and the inhibitor are shown in salmon) or **9** (carbon atoms for highlighted protein residues and the inhibitor are shown in light blue). In all other panels, carbon atoms for highlighted protein residues are colored blue and ligand carbon atoms are shown in yellow.

To alleviate these steric effects and take advantage of the hydrogen-bonding capacity of Gln31 within the glycerol pocket of MabDHFR, we replaced the *n*-pentyl moiety in **3** with a *n*-hydroxybutyl. The resulting compound, **4**, was ~2-fold more potent to all three enzymes. The co-crystal structure of MulDHFR complexed to NADP and **4** showed that the inhibitor's hydroxyl moiety participated in a hydrogen bonding network involving water molecules and the side chain of a conserved aspartate residue (Asp29/Asp30/Asp31 in Mul-, Mab- and MavDHFR, respectively) (**Figure 4B**). The structure also suggested the hydroxyl moiety in **4** would be within hydrogen bonding distance to side chain atoms from Gln31 in MabDHFR. Nevertheless, as introduction of the hydroxyl group resulted in similar potency gains for all three enzymes, it is unlikely that the improvement observed for the MabDHFR was due to this particular interaction. Together, these results further indicated that substitutions in **P218** ethyl group modulated compound potency and selectivity.

We next explored the effect of replacing the ethyl group in **P218** with alkoxy moieties, yielding compounds **5-7**. This strategy was motivated by the expectation that the oxygen atom in these molecules are within hydrogen bond distance to side chain atoms of the same conserved aspartate residue shown to interact with the hydroxyl moiety in **4** (Asp29/Asp30/Asp31 in Mul-, Mab and MavDHFR, respectively). However, all alkoxy containing compounds were inactive towards the NTM and human enzymes (K_i > 1250 nM). The lack of activity of these compounds was likely due to electronic effect of the alkoxy group in the pyrimidine ring, thus reducing the strength of the polar interactions that anchor **P218**'s DAP within the enzyme's ligand-binding site. Additionally, the presence of a hydrogen bond acceptor deep into the enzyme's glycerol pocket, which is mostly composed of hydrophobic residues, may not be favored.

Thus far, the use of linear moieties in place of **P218**'s ethyl group has not led to significant reductions in potency towards the human enzyme. Moreover, similar potency reductions were also seen for the mycobacterial enzymes. To improve the selectivity of our compounds towards the mycobacterial enzymes, we next explored the use of bulkier moieties by replacing **P218**'s ethyl group with non-aromatic (analogue **8**) and aromatic (analogue **9**) ring structures. Compared to

16

P218, compound **8** featuring a cyclohexyl group was equipotent towards both *M. abscessus* and *M. avium* enzymes, whereas the compound was inactive on the human enzyme (K_i > 1250 nM). Conversely, the phenyl ring in **9** was much better tolerated by MavDHFR (<2-fold potency drop) than by MabDHFR (~20-fold potency drop) or the human enzyme (~20-fold potency drop). The co-structure of MulDHFR complexed to **9** and NADP showed the inhibitor's phenyl moiety sandwiched between the side chain residues of Asp29 and Leu30 from one side and that of Ile22 from the other side (**Figure 4C**). The Leu to Gln substitution in the glycerol pocket of MabDHFR may explain the larger reduction in potency of this compound towards the *M. abscessus* enzyme, likely due to a combination of decreased hydrophobicity, increased polarity, and steric hindrance. The co-structure of MulDHFR bound to **8** further highlighted these points (**Figure 4C**). It showed that the less planar cyclohexyl group in **8** adopted a slightly different orientation than the phenyl ring in **9** (relative ring rotation of ~30 degrees), which may explain why **8** is equally well tolerated by both *M. abscessus* and *M. avium* enzymes. Together, these results suggested that both steric bulk and electronic properties of substituents of the ethyl group in **P218** are critical in determining binding potency and enzyme selectivity of DHFR inhibitors.

Building on these results, we aimed to increase the steric bulk and modify the electronic properties of the aromatic ring in **9** by appending either a CF_3 or a methoxy group, resulting in compounds **10-15**. These modifications significantly reduced compound activity towards the human enzyme, with compounds **10-13** exhibiting K_i values > 1250 nM against HsaDHFR. The lack of activity towards the human enzyme was likely due to a combination of electronic and steric effects, as the bulkier rings may clash with the phenylalanine residue unique to the human enzyme (Phe31 in HsaDHFR). In this series, compound **14** was ~2-fold more potent than **P218**, whereas **15** was ~6-fold less active than the parent compound towards the human enzyme. Notably, **11** and **12**, with a CF_3 substituent in equivalent positions, were inactive towards the human enzyme, underscoring our hypothesis that both steric bulk and electronic properties are crucial in determining binding potency for the human enzyme.

Likewise, the incorporation of a bulkier, strong electron-withdrawing CF_3 group into the phenyl ring of **9** markedly diminished the binding affinity of compounds to both NTM enzymes, with potency reductions ranging from 2.5- to ~270-fold relative to **9**. The magnitude of this effect depended on the position of the CF_3 group and the identity of the mycobacterial enzyme. Overall, a CF_3 group in the *ortho*-position (analogue **10**) was the most well-tolerated substitution and showed only small potency reductions for both NTM - 4-fold for MavDHFR and 2.5-fold for MabDHFR. In contrast, compounds having CF_3 in *meta*- (analogue **11**) or *para*- (analogue **12**) position were much less tolerated. Co-crystal structures of MulDHFR bound to each one of the three CF_3-containing derivatives showed this moiety explored different regions of the enzyme glycerol pocket depending on their placement in the benzene ring (**Figures 4D-F**). Based on these co-crystal structures, the presence of the bulkier side chain from Gln31 in MabDHFR may explain the enzyme low tolerance towards compounds with CF_3 groups in *meta*- and *para*- positions due to steric effects. However, the large drop in potency observed for these compounds towards the *M. avium* enzyme is harder to rationalize based on steric effects alone. Together, our data indicated replacing the ethyl group in **P218** with trifluoromethylphenyl moieties could differentially affect the potency of inhibitors towards the human and NTM enzymes, with these compounds being particularly inactive towards the human enzyme.

In contrast, addition of a methoxy group to different positions in the phenyl ring of **9** (analogues **13-15**) was, in general, better tolerated by the NTM enzymes than the compounds having trifluoromethylphenyl moieties. Once again, compound activity depended on the position of the methoxy group within the phenyl ring and the identity of the DHFR enzyme. Notably, compound **15** with a *para*-methoxy group maintained equivalent potency to **9** for both NTM enzymes. Nevertheless, **15** was also active towards the human enzyme, albeit at least 400-fold less potent towards the human enzyme compared to the NTM enzymes. Surprisingly, **13**, featuring a methoxy group in the *ortho*-position, was the least tolerated among the methoxy-containing compounds, contrasting with the observed tolerance for *ortho*-CF_3-substituted compounds. This discrepancy further emphasizes the critical role of substituent positioning and electronic effects for

compound activity. The co-crystal structures of NADP-bound MulDHFR in complex with **14** and **15** revealed the methoxy groups of these compounds occupied equivalent positions in the glycerol pocket compared to the corresponding CF_3 substituents in **11** and **12 (Figures 4G,H)**. However, two significant differences were noted. First, the oxygen atoms in the methoxy moieties of **14** and **15** formed hydrogen bonds to water molecules found in the enzyme's glycerol pocket. Second, the phenyl ring attached to the *para*-methoxy group in **15** was rotated ~80 degrees compared to the equivalent moieties in **9** and **12**. These findings highlighted that compound flexibility is yet another important factor determining activity towards DHFR.

Our last series of analogues (**16-18**) explored the use of amines to replace the ethyl moiety in **P218**. All compounds with amine substitutions were inactive towards the human enzyme (K_i > 1250 nM), providing yet another strategy to achieve selectivity in our NTM DHFR inhibitors. Introduction of a *n*-propylamine (**16**) reduced compound potency by > 60-fold to both NTM DHFRs compared to compound **2** having an *n*-propyl group. Introducing a secondary amine to the cyclohexyl moiety of **8** (analogue **17**) reduced potency 10- and 350-fold towards MavDHFR and MabDHFR, respectively. Finally, compound **18** having an amine added to the aromatic ring of **9** was better tolerated by both enzymes, having 2.5- and 4.5-fold reduced potency to MavDHFR and MabDHFR, respectively. Together, these results further confirmed that both shape and electronic properties of the substituent influenced binding affinity differently to each one of the two NTM DHFR. Specifically, compounds **16** and **17** have amine groups with similar basicity, but the ring structure of **17** is 6-fold more potent than the linear structure in **16** towards the MavDHFR. On the other hand, compounds **16** and **17** are equipotent towards MabDHFR. Similarly, the low basicity of the pyridine ring in **18** was better tolerated by MavDHFR than by MabDHFR.

In conclusion, our enzyme activity and structural data indicated that modifications to **P218** ethyl group can explore different aspects of the glycerol pocket found in the mycobacterial enzymes. Although our compounds did not improve on **P218** *in vitro* activity towards the NTM enzymes, we were able to generate novel DHFR inhibitors that were virtually inactive towards the human

enzyme. Importantly, despite the high amino acid conservation within the "glycerol pockets" of the two NTM DHFRs, our results suggested that the substitution of Leu32 in MavDHFR with Gln31 in MabDHFR had a major impact on compound potency. This is illustrated by the differential effect observed for compounds having bulkier and more polar moieties.

Chemistry.

For the preparation of **P218** as well as the alkyl and aryl analogues, we took advantage of the metalation reaction of the pyrimidine ring in intermediates **19** as previously described.[44] Metalation of the 2,4-dichloro-5-alkoxy pyrimidines with $(TMP)_2Zn·2MgCl_2·2LiCl$ accompanied by Pd-catalyzed reaction led to the desired modification at the C-6 position. We used Negishi, Suzuki, and Sonogashira couplings as tools to modify the C-6 position (**Scheme 3**). The double bonds were hydrogenated in the presence of Adam's catalyst, followed by S_NAr reaction to introduce 2,4-dimethoxybenzylamine in the pyrimidine ring. A final deprotection step in the presence of trifluoroacetic acid (TFA) and anisole afforded **P218** and analogues **1**-**4** and **8**-**18**. The preparation of the alkoxy analogues (compounds **5**-**7**) employed a different route and is described in the Supplementary Information.

20

Scheme 1. Synthetic route to access **P218** analogues containing modification at C-6 position.[a]
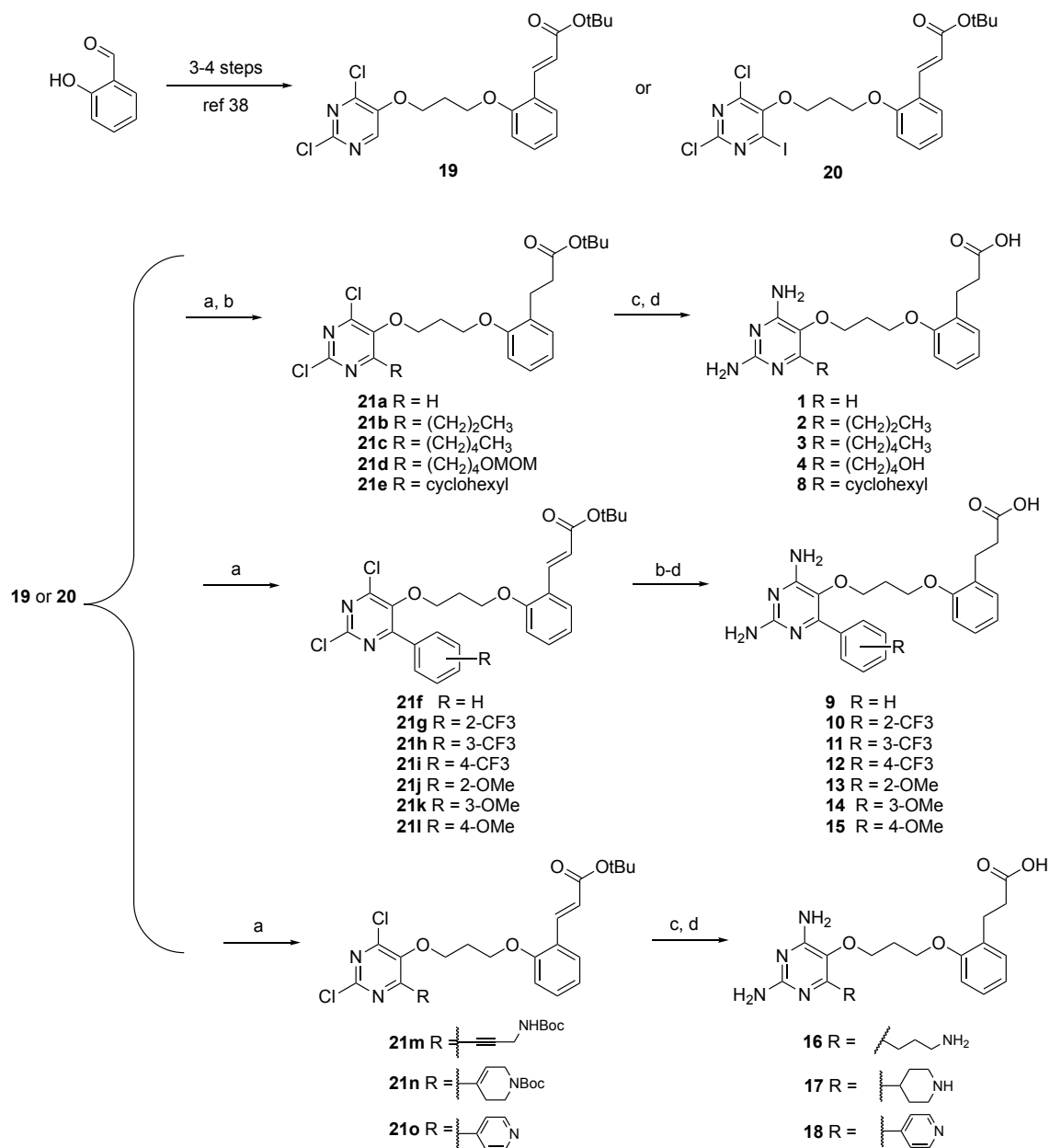
[a] Reagents and Conditions: (a) For Negishi reaction: $(TMP)_2Zn·2MgCl_2·2LiCl$, THF, 25°C, 2 h, then $Pd(dba)_2$, $P(o\text{-furyl})_3$, and coupling partner; for Sonogashira reaction: $Pd(PPh_3)Cl_2$, CuI, DIPEA, coupling alkyne, DMF, r.t; for Suzuki reaction: $Pd(dppf)Cl_2$, K_3PO_4, THF:H2O (10:1), and boronic ester, 70°C. (b) PtO_2, 1 atm. H_2, EtOAc. (c) 2,4-dimethoxybenzylamine, 120 °C. (d) TFA, anisole, 48 h, r.t..

Activity of **P218** derivatives on *M. abscessus* and *M. avium*.

We next evaluated the ability of selected **P218** analogues to inhibit the growth of *M. abscessus* and *M. avium* in culture. In these assays, we used amikacin, an aminoglycoside antibiotic, as a positive control. This drug binds to the 30S subunit of the bacterial ribosome, inhibiting protein translation, [45] and has been used since the 1990's to treat NTM infections.[15] Overall, our data confirmed our previous observations that *M. avium* is much more sensitive to **P218** analogues than *M. abscessus* (**Table 2**). Out of the 10 **P218** analogues tested, 6 were more potent towards *M. avium* than amikacin, whereas only one was more potent than this antibiotic towards *M. abscessus*. Some of our novel **P218** analogues were also more potent than the parent compound against *M. avium* and *M. abscessus*. Specifically, **4**, **8** and **15** were more active than **P218** and amikacin against *M. avium*; whereas **8** was more potent than **P218** and amikacin against *M. abscessus*.

TABLE 2

Table 2 – Whole cell activity of selected compounds in *M. avium* and *M. abscessus*

Compound	*M. avium* MIC [a] (µg/mL)	*M. abscessus* MIC [a] (µg/mL)
Amikacin	1.7 (1.5-1.9)	2.1 (1.9-2.5)
P218	0.3 (0.2-0.5)	28 (18-37)
3	0.6 (0.2-3.3)	ND
4	0.1 (0.1-0.1)	77 (66-93)
8	0.1 (0.0-0.2)	1.5 (1.0-2.4)
9	0.3 (0.2-0.5)	ND
10	3.6 (2.7-4.8)	ND
14	5.6 (3.8-8.2)	ND
15	0.2 (0.1-0.3)	ND
16	13 (9-20)	ND
17	6.2 (4.2-8.8)	ND
18	0.6 (0.4-1.0)	ND

[a] Data shown are mean and CI 95 % (in parenthesis) for three biological replicates. ND – growth inhibition $\leq$ 75 % at the highest compound concentration used. Dose-response curves used for MIC calculation can be found in Supplementary Figures S2 and S3.

Bacteria in general, and mycobacteria in particular, have a cell envelope that is virtually impregnable to antibiotics.[12,46] Thus, compounds with *in vitro* activity against purified enzymes may not be effective against the bacteria in culture.[47] Nevertheless, for *M. avium*, we noticed a linear relationship between compound activity *in vitro* and in cell-based assays (R^2 = 0.84; **Figure 5**). Interestingly, data from matched pairs of compounds (**3** vs. **16**; **8** vs. **17**; **9** vs. **18**) suggested addition of primary, secondary, or aromatic amines was detrimental to cell-based activity. These results contrasted with previous work in Gram-negative bacteria showing the presence of amines can increase compound permeability.[48] Our data also indicated that replacing **P218** ethyl moiety with a hydroxyalkyl (**4**) or a cyclohexyl (**8**) group lead to greater than expected improvements in cell-based activity.

In conclusion, data from cell-based assays identified novel **P218** derivatives that are more effective against *M. avium* and *M. abscessus* in culture than amikacin, an antibiotic in clinical use against NTM infections, and the parent compound **P218**.

24

FIGURE 5

Compound activity
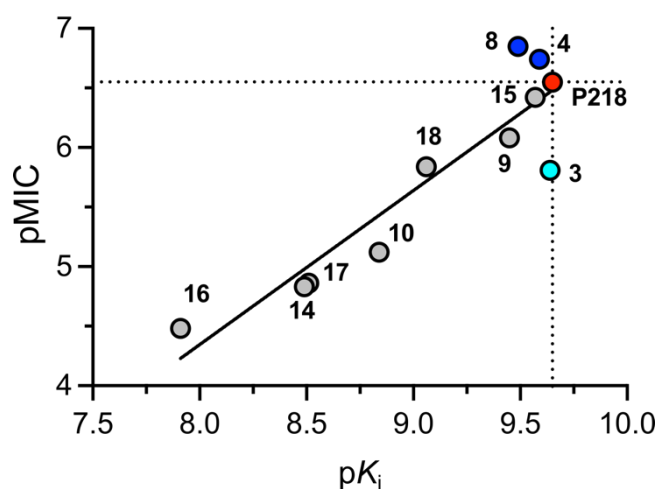**(MavDHFR *in vitro* vs. *M. avium* whole cells)**

Figure 5 – Correlation of compound activity in MavDHFR enzymatic assays (x-axis) and in *M. avium* whole cell phenotypic assays (y-axis). Dashed black lines indicate the (x,y) coordinates for **P218** (red circle). Compounds with higher-than-expected activity in phenotypic assays (**4** and **8)** are highlighted in dark blue, whereas compound **3** with lower-than-expected phenotypic activity is highlighted in cyan. Linear regression (black solid line - R^2 = 0.84) for all shown datapoints was obtained using Prism (v.10).

DMPK profiling of novel **P218** analogues.

Compounds **4, 8, 9**, and **15** showed promising activity against *M. avium* (MIC < 1 μM) and demonstrated higher selectivity towards the NTM enzyme than **P218**. Therefore, they were next profiled in DMPK studies to identify their solubility and metabolic stability in hepatocytes and microsomes from both human and mouse (**Table 3**). These analyses revealed that replacement of **P218** ethyl group with more hydrophobic moieties, such as cyclohexyl (analogue **8**) and phenyl (analogues **9** and **15**), decreased compound solubility compared to **P218**. On the other hand, compound **4** having a hydroxyl moiety had comparable solubility to **P218**. Nevertheless, all tested **P218** analogues had solubility greater than 10 μM, which is within the desired range for a lead compound in infectious diseases.[49] We also tested compound permeability in Madin-Darby canine kidney (MDCK) cells. In these analyses, all but one of the tested compounds were more cell permeable than **P218** and had apparent permeability parameters within the desired range for antibiotics (Papp > 10 nm/sec).[50] The exception was **4,** the analogue with the hydroxyl moiety. These results were not unexpected, as the addition of hydrophobic groups is expected to reduce solubility and the addition of polar groups to reduce compound permeability to mammalian cells. Additionally, all tested **P218** analogues demonstrated excellent metabolic stability in both mouse and human liver microsomes and hepatocytes.

TABLE 3

<table>
<tr><th colspan="7">Table 3 – <i>In vitro</i> DMPK properties of selected compounds</th></tr>
<tr><th rowspan="3">Compound</th><th rowspan="3">Sol.^a
(μM)</th><th rowspan="3">MDCK Papp^b
(nm/sec)</th><th colspan="4">Intrinsic clearance</th></tr>
<tr><th colspan="2">Microsomes
(mL/min/g liver)</th><th colspan="2">Hepatocytes
(mL/min/g liver)</th></tr>
<tr><th>Mouse^c</th><th>Human^d</th><th>Mouse^e</th><th>Human^f</th></tr>
<tr><td>P218</td><td>233</td><td>30</td><td>< 0.5</td><td>< 0.4</td><td>< 0.76</td><td>< 0.66</td></tr>
<tr><td>4</td><td>227</td><td>8</td><td>< 0.5</td><td>< 0.4</td><td>< 0.76</td><td>< 0.66</td></tr>
<tr><td>8</td><td>43</td><td>32</td><td>< 0.5</td><td>0.54</td><td>2.2</td><td>< 0.66</td></tr>
<tr><td>9</td><td>51</td><td>54</td><td>1.3</td><td>0.43</td><td>2.2</td><td>< 0.66</td></tr>
<tr><td>15</td><td>67</td><td>41</td><td>< 0.5</td><td>< 0.4</td><td>0.59</td><td>< 0.66</td></tr>
</table>

[a] Solubility; [b] Madin-Darby canine kidney cells apparent permeability; scaling factors: [c] - 48 mg protein/g liver; [d] - 39.7 mg protein/g liver; [e] - 135 x 10⁶ cells/g liver; [f] - 118 x 10⁶ cells/g liver.

In vivo profiling of compound **8**.

These results encouraged us to profile the pharmacokinetics of **8** in mice. The compound was dosed at 1 mg/kg intravenously (IV) and 3 mg/kg orally (PO) to female BALB/c mice. The level of the parent compound was monitored over 24 h (**Figure 6; Table 4**). In line with the *in vitro* clearance data, we observed low clearance for **8** *in vivo* following IV dosing, with a half-life ($t_{1/2}$) of 0.5 h. Additionally, PO dosing indicated that **8** was likely subjected to first pass effects, reaching a maximal concentration (C_{max}) of 279 ng/mL. The compound $t_{1/2}$ following PO dosing was 2.5 hours and bioavailability (F) ~40 %. We also determined **8** protein plasma binding (PPB) and found that the fraction of unbound compound in plasma (f_u) to be ~0.02. These results indicated that, to reach free plasma concentrations of **8** equivalent to the MIC value observed against *M. avium* in culture (60 ng/mL) would require dosing the compound at ~300 mg/kg in mice – assuming linearity upon dose scale-up. Thus, despite the promising DMPK properties of this compound, we chose not to continue with further pre-clinical tests at this point.
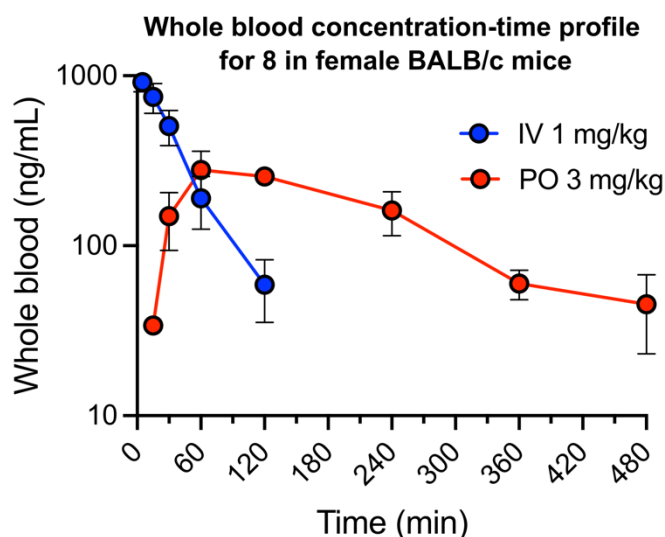
FIGURE 6

Figure 6 – *In vivo* profiling of **8** in female BALB/c mouse. Whole blood compound concentration was determined at indicated time points following a single intravenous (at 1.0 mg/kg; IV – blue circles or oral (at 3.0 mg/kg; PO – red circles) administration. Data points shown are mean $\pm$ SEM (n=3) for **8** whole blood concentration. Solid colored lines are shown as visual guides.

TABLE 4

Table 4 – Pharmacokinetics parameters of 8 in female BALB/c mouse						
Administration	**AUC$_{last}$** (min×ng/mL)	**AUC$_{INF\_pred}$** (min×ng/mL)	**AUC$_{Extrap}$** (%)	**Cl$_{obs}$** (mL/min/kg)	**Vss$_{obs}$** (L/kg)	**Half-life** (h)
IV (1 mg/kg)	40,507	42,750	5	23	0.9	0.5
	AUC$_{last}$ (min×ng/mL)	**AUC$_{INF\_pred}$** * (min×ng/mL)	**AUC$_{Extrap}$** * (%)	**C$_{max}$** (ng/mL)	**T$_{max}$** (min)	**F** (%)
PO (3 mg/kg)	49,232	-	-	279	30	41

* AUC$_{INF\_pred}$ not reported for PO as AUC$_{extrap}$ >20 %

Conclusions

Here we present an extensive SAR exploration of the glycerol pocket of the DHFR enzyme from *M. abscessus* and *M. avium*, two emerging human pathogens that cause recurrent lung infections in immunocompromised patients. Our results demonstrated that the DHFR glycerol pocket can be targeted to achieve selectivity versus the human enzyme. However, despite the high level of similarity between the glycerol pockets of the two NTM enzymes, developing compounds that were potent against both DHFRs proved challenging. Our work highlighted the importance of residue Gln31 in the glycerol pocket of MabDHFR for achieving compound potency. With the aid of structural information, we identified compounds that were inactive against the human enzyme, yet maintained potent activity against both NTM DHFRs. Notably, some of our **P218** analogues exhibited potent antimicrobial activity against both NTMs, with analogue **8** showing activity comparable to amikacin in *M. abscessus* and considerably greater potency than this antibiotic in *M. avium*. Our studies further reinforced that treating *M. abscessus* is particularly challenging, likely due to the presence of an extensive set of efflux pumps in this bacterium. Moreover, our most potent **P218** analogues displayed improved DMPK profiles compared to the parent compound, particularly in terms of solubility and microsome stability. Future work will focus on enhancing the bioavailability of **8** and conducting detailed *in vivo* studies to understand its distribution in mice.

Experimental Section

Chemistry. All starting materials and reagents were of commercial quality and were used without further purification. Compounds **19**, **20**, **21a**, **2**, **4**, **8**, **9**, **16**, and **17** were prepared according to previous procedure.[44] All reactions were carried out with freshly distilled solvents, using anhydrous conditions unless otherwise noted. DCM and Et_3N were distilled over calcium hydride. THF was distilled over metallic Na and benzophenone. DMF was obtained in anhydrous grade and was used without previous treatment. The sealed tubes used in the cross-coupling reactions were previously dried in an oven for at least 3 h. Other reagents were obtained from commercial sources and were used without prior purification. The reactions were monitored by thin-layer chromatography (silica gel 60 F254 in aluminum foil, Merck). Silica gel 200–400 mesh was used for flash column chromatography.

TMPMgCl·LiCl was purchased from Merck as a 1M solution in THF. The base was titrated with benzoic acid (triplicate) using 4-(phenylazo)diphenylamine as an indicator affording ca. 0.8M solution.

1M $ZnCl_2$ solution: A Schlenk-Flask was charged with $ZnCl_2$. The solid was carefully melted using a heating gun under vacuum, and the process was repeated three times. After cooling to r.t., dry THF was added, and the mixture was stirred until the solid was dissolved.

$TMP_2Zn·2MgCl_2·2LiCl$: Freshly titrated TMPMgCl·LiCl (1 equiv.) was added dropwise to a 1M solution of $ZnCl_2$ in THF (0.5 equiv.) in a Schlenk-Flask under nitrogen atmosphere. The solution was covered with aluminum foil and stirred at r.t. for 18h before titration with benzoic acid using 4-(phenylazo)diphenylamine as an indicator.

NMR spectra were recorded on a Bruker Avance III HD 250 MHz, Bruker Avance III 400 MHz, or a Bruker Avance III 500 MHz and processed using MestreNova 12.0.4 software. The chemical shifts are reported in parts per million (ppm) on a delta (δ) scale. The residual solvent peaks were used as reference values; for ^1H NMR, $CHCl_3$ = 7.26 ppm, CH_3OH = 3.31, $(CH_3)_2SO$ = 2.50 ppm; for ^{13}C NMR, $CDCl_3$ = 77.16 ppm, CD_3OD = 49.00 ppm, or $(CD_3)_2SO$ = 39.52. Signal multiplicity was

reported as singlet (s), doublet (d), triplet (t), quartet (q), quintet (quint.), and multiplet (m). High-resolution mass spectra (HRMS) were acquired on an Orbitrap Thermo QExactive Mass Spectrometer, using electrospray ionization (ESI). Infrared (IR) spectra were recorded using a Thermo Scientific Nicolet IS5 spectrometer using Thermo Scientific ID3 ATR, and the absorption frequencies are reported in cm^{-1}.

The purity of final compounds was determined via high-performance liquid chromatography (HPLC) using an Agilent 1100 Series LC system (Agilent Technologies, Santa Clara, CA) with a Phenomenex Kinetex C8 100A column (150 mm × 4.6 mm, 2.6 µm) (Phenomenex Inc., Torrance, CA), and detection was performed with a UV DAD at wavelengths of 254 and 280 nm. The mobile phase solvent A was 0.1 % Formic acid (FA) in water, and solvent B was 0.1 % FA in 100 % Acetonitrile (ACN). The sample (10 µL) was loaded at a flow rate of 400 µL/min, and eluted from the C18 column at a flow rate of 500 µL/min with the following gradient step: from 5 to 95 % solvent B over 6.5 min. The column was regenerated by washing at 95 % solvent B for 2.5 min and re-equilibrated at 5 % solvent B for 3 min. Final compounds showed a purity of >95 % according to their respective peak areas at 254 nm.

General Procedure A *(Suzuki-Miyaura cross-coupling)*. In a dry, nitrogen-flushed test tube equipped with a magnetic stirring bar and a septum were added the iodopyrimidine (1 equiv.), the boron species (2 equiv.), Pd(dppf)Cl$_2$ (5 mol%) and K$_3$PO$_4$ (2 equiv.). Then, a mixture of THF (previously degassed with N$_2$ for 15 min): water (10:1) was added (final concentration 0.1M), and the mixture was stirred at 80 ºC for 36 h. After cooling to r.t., water was added, and the aqueous layer was extracted with diethyl ether. The combined organic layers were washed with brine, dried over Na$_2$SO$_4$, filtered, and the solvent was removed under reduced pressure. The product was purified by column chromatography on silica gel.

General Procedure B *(hydrogenation reactions)*. The pyrimidine (1 equiv.) was dissolved in ethyl acetate (0.1 M) under a N$_2$ atmosphere. PtO$_2$ (20 mol%) was added, and the reaction was purged with H$_2$. The mixture was allowed to stir at room temperature and monitored by TLC. If the conversion stopped, an additional PtO$_2$ (20 mol%) was added, and the mixture was stirred and monitored until complete conversion of the starting material. Then, the material was filtered over Celite using ethyl acetate as eluent, and the solvent was removed under reduced pressure.

32

General Procedure C *(S$_N$Ar reaction + deprotections with TFA and anisole)*. Step 1. The corresponding 2,4-dichloropyrimidine (1 equiv.) and 2,4-dimethoxybenzylamine (10 equiv.) were added to a sealed tube purged with N$_2$, and the mixture was stirred at 120 °C for 60 h. The product was dissolved in ethyl acetate (5 mL), the solution was transferred to a round bottom flask, and the solvent was evaporated. Then, the product was purified by column chromatography on silica gel. Step 2. A 20 mL culture tube was charged with the material from the previous step (1 equiv.) and a magnetic stirring bar under nitrogen. Then, anisole (10 equiv.) was added, followed by the addition of TFA (43 equiv.). The vial was sealed and stirred at room temperature for 20h. The solvent was evaporated, and the product was purified by reverse-phase chromatography using Biotage [(Biotage® SNAP Ultra C18 with HP-sphere 25 μm 12 g), gradient elution from 10 % to 100 % ACN in water (with 0.1 % TFA)]. The material was transferred to a 20 mL culture tube using methanol (5 mL). The solvent was evaporated, and 1M NaOH solution was added dropwise to solubilize the material (pH 13). Then, acetic acid was added dropwise until precipitation of a white solid (pH 5). The solid was collected by filtration, then suspended in water (2 mL), and sonicated to remove sodium trifluoroacetate contaminant. The water was removed by syringe, followed by the addition of water (1 mL) and filtration.

General Procedure D *(Sonogashira cross-couplings)*. In a dry, nitrogen-flushed test tube equipped with a magnetic stirring bar and a septum were added the corresponding iodopyrimidine (1 equiv.), Pd(II)(PPh$_3$)$_2$Cl$_2$ (5 mol%), and CuI (15 mol%). Then, DMF (0.1 M), previously degassed for 15 min with N$_2$, was added to the mixture, followed by *N,N*-diisopropylethylamine (3 equiv.) and the alkyne (1.1 equiv.). The resulting mixture was stirred at room temperature for 4 h. The reaction was then diluted with ethyl acetate (10 mL), and the organic layer was washed with water (5 x 10 mL). The organic layer was dried over Na$_2$SO$_4$, filtered and the solvent was removed under reduced pressure, and the product was purified by column chromatography.

General Procedure E *(Negishi cross-couplings)*. A dry, nitrogen-flushed test tube equipped with a magnetic stirring bar and a septum was charged with pyrimidine (1 equiv.) and THF (0.5 M). (TMP)$_2$Zn·2MgCl$_2$·2LiCl solution (0.6 equiv.)

was added dropwise, and the reaction mixture was stirred at 25 °C for 2h. Then, a solution of the halide or triflate (1.2 equiv.), Pd(dba)$_2$ (5 mol%) and tri-(2-furyl)phosphine (10 mol%) in dry THF (0.2 mL) under N$_2$ was canulated to the reaction flask. The mixture was stirred at 70 °C for 3h. The solution was neutralized with sat. aq. solution of NH$_4$Cl and extracted with diethyl ether. The combined organic layers were dried over Na$_2$SO$_4$, filtered, and the solvent was removed under reduced pressure. The product was purified by column chromatography.

tert-Butyl 3-(2-(3-((2,4-dichloro-6-pentylpyrimidin-5-yl)oxy)propoxy)phenyl)propanoate (21c). **General procedure D** was used with pyrimidine **20** (200 mg, 0.363 mmol, 1 equiv.), Pd(II)(PPh$_3$)$_2$Cl$_2$ (12.7 mg, 0.0181 mmol, 5 mol%), CuI (10.6 mg, 0.0544 mmol, 15 mol%), DMF (3.6 mL), *N,N*-diisopropylethylamine (190 µL, 1.09 mmol, 3 equiv.), and 1-pentyne (61.9 mg, 0.399 mmol, 1.1 equiv.). Purification by flash column chromatography on silica gel [(20 mm x 35 mL, H=14 cm of SiO$_2$), gradient elution from 10 to 30 % ethyl acetate in hexane, 10 % increases, 100 mL runs] gave a beige oil (142 mg, 0.246 mmol, 68 % yield).

Pyrimidine **21c** was prepared according to **General procedure B**, using the material from the previous step (60.0 mg, 0.122 mmol, 1 equiv.), ethyl acetate (1.2 mL), and PtO$_2$ (6.3 mg, 0.024 mmol, 20 mol%). The reaction took 2 h to complete, and purification by column chromatography [(15 mm x 15 mL, H=16 cm of SiO$_2$), gradient elution from 10 to 20 % ethyl acetate in hexane, 5 % increases, 30 mL runs] afforded **21c** (34.0 mg, 0.068 mmol, 56 % yield) as a colorless oil. **^{1}H NMR (250 MHz, CDCl$_3$)** δ 7.24 – 7.10 (m, 2H), 6.95 – 6.79 (m, 2H), 4.22 (dt, *J* = 7.9, 5.9 Hz, 4H), 2.89 (dd, *J* = 8.7, 6.9 Hz, 2H), 2.80 – 2.66 (m, 2H), 2.49 (dd, *J* = 8.7, 6.9 Hz, 2H), 2.33 (quint, *J* = 5.9 Hz, 2H), 1.66 (quint, *J* = 7.6 Hz, 2H), 1.40 (s, 9H), 1.23 (qd, *J* = 8.2, 7.0, 4.5 Hz, 4H), 0.84 (t, *J* = 6.8 Hz, 3H). **^{13}C NMR (63 MHz, CDCl$_3$)** δ 172.7, 169.5, 156.5, 155.4, 153.4, 147.3, 130.1, 129.1, 127.6, 120.8, 110.9, 80.3, 71.0, 63.5, 35.6, 32.4, 31.7, 30.2, 28.2, 28.0, 26.2, 22.5, 14.0. **v$_{max}$ (cm^{-1}, thin film, ATR)**: 2963, 2932, 1730, 1545, 1526, 1496, 1456, 1403, 1368, 1344, 1243, 1149, 1113, 1053, 985, 954, 849, 794, 752. **HRMS (ESI+/TOF) m/z:** calc. for [C$_{25}$H$_{34}$Cl$_2$N$_2$O$_4$+H]$^+$ 497.19684, found 497.19674.

tert-Butyl **(E)-3-(2-(3-((2,4-dichloro-6-(2-(trifluoromethyl)phenyl)pyrimidin-5-yl)oxy)propoxy)phenyl)acrylate (21g)**. Pyrimidine **21g** was prepared according to **General procedure A**, using **20** (80.0 mg, 0.145 mmol, 1 equiv.), 2-(trifluoromethyl)phenylboronic acid (30.3 mg, 0.160 mmol, 2 equiv.), Pd(dppf)Cl$_2$ (5 mg, 0.007 mmol, 5 mol%), K$_3$PO$_4$ (63 mg, 0.29 mmol, 2 equiv.), THF (1.3 mL), and water (130 µL). The product was purified by column chromatography on silica gel [(20 mm x 50 mL, H=21 cm of SiO$_2$), gradient elution from 5 to 15 % ethyl acetate in hexane, 5 % increases, 100 mL runs] to give **21g** (50 mg, 0.14 mmol, 61 % yield) as a colorless oil. **^{1}H NMR (250 MHz, CDCl$_3$)** δ 7.74 (d, J = 16.1 Hz, 1H), 7.61 (d, J = 7.8 Hz, 1H), 7.55 – 7.27 (m, 5H), 6.96 (t, J = 7.5 Hz, 1H), 6.69 (d, J = 8.3 Hz, 1H), 6.33 (d, J = 16.1 Hz, 1H), 3.94 (t, J = 5.6 Hz, 2H), 3.85 (t, J = 5.8 Hz, 2H), 2.04 (quint, J = 5.9 Hz, 2H), 1.52 (s, 9H). **^{19}F NMR (235 MHz, CDCl$_3$)** δ -57.80. **^{13}C NMR (63 MHz, CDCl$_3$)** δ 166.8, 162.9, 157.1, 156.7, 153.0, 147.1, 138.5, 132.0 (q, J = 2.0 Hz), 131.6, 131.2, 130.3, 130.2, 128.7 (q, J = 31.5 Hz), 128.4, 127.0 (q, J = 4.7 Hz), 123.6 (d, J = 274.1 Hz), 123.6, 120.9, 120.4, 111.9, 80.4, 70.4, 63.6, 29.6, 28.3. **v$_{max}$ (cm^{-1}, thin film, ATR)**: 2975, 1703, 1630, 1599, 1524, 1491, 1456, 1404, 1369, 1340, 1315, 1273, 1247, 1149, 1119, 1051, 1037, 985, 951, 876, 828, 756, 660. **HRMS (ESI+/TOF) m/z:** calc. for [C$_{27}$H$_{25}$Cl$_2$F$_3$N$_2$O$_4$+H]$^+$ 569.12162, found 569.12226.

tert-Butyl **(E)-3-(2-(3-((2,4-dichloro-6-(3-(trifluoromethyl)phenyl)pyrimidin-5-yl)oxy)propoxy)phenyl)acrylate (21h)**. Pyrimidine **21h** was prepared according to **General procedure E**, using **19** (60.0 mg, 0.141 mmol, 1 equiv.), (TMP)$_2$Zn·2LiCl·2MgCl$_2$ (385 µL, 0.0846 mmol) (0.22 M in THF, 0.6 equiv.), Pd(dba)$_2$ (4.1 mg, 0.0071 mmol, 5 mol%), P(o-furyl)$_3$ (3.3 mg, 0.0141 mmol, 10 mol%), 3-iodobenzotrifluoride (46 mg, 0.17 mmol, 1.2 equiv.), and THF (0.28 mL). The product was purified by column chromatography on silica gel [(20 mm x 50 mL, H=23 cm of SiO$_2$) gradient elution from 5 to 15 % ethyl acetate in hexane, 5 % increases, 100 mL runs] to give a colorless oil (57 mg, 0.10 mmol, 71 % yield). **^{1}H NMR (250 MHz, CDCl$_3$)** δ 8.3 (dq, J = 1.9, 0.9 Hz, 1H), 8.2 – 8.1 (m, 1H), 7.8 (d, J = 16.2 Hz, 1H), 7.7 – 7.6 (m, 1H), 7.5 – 7.3 (m, 3H), 7.1 – 6.9 (m, 1H), 6.8 (dd, J = 8.4, 1.1 Hz, 1H), 6.3 (d, J = 16.1 Hz, 1H), 4.1 (t, J = 5.9 Hz, 2H), 4.1 (t, J = 5.8 Hz, 2H), 2.2 (quint, J = 5.8 Hz, 2H), 1.5 (s, 9H). **^{13}C NMR (63 MHz, CDCl$_3$)** δ 166.7, 160.0, 157.9, 157.0, 153.9, 147.0, 138.3, 134.3, 132.6, 131.3, 131.3 (q, J = 32.8 Hz), 129.3,

128.4, 127.9 (q, J = 3.6 Hz), 126.4 (q, J = 3.7 Hz), 123.8 (d, J = 272.1 Hz), 121.1, 120.5, 112.0, 80.4, 71.0, 63.9, 29.8, 28.3. **^{19}F NMR (235 MHz, CDCl$_3$)** δ -62.68. **ν$_{max}$ (cm^{-1}, thin film, ATR)**: 2981, 1705, 1631, 1600, 1538, 1522, 1489, 1457, 1402, 1368, 1343, 1324, 1253, 1151, 1131, 1104, 1075, 1051, 986, 892, 791, 756, 699, 668. **HRMS (ESI+/TOF) m/z:** calc. for $[C_{27}H_{25}Cl_2F_3N_2O_4+H]^+$ 569.12162, found 569.12145.

tert-Butyl (E)-3-(2-(3-((2,4-dichloro-6-(4-(trifluoromethyl)phenyl)pyrimidin-5-yl)oxy)propoxy)phenyl)acrylate (21i). Pyrimidine **21i** was prepared according to **General procedure E**, using **19** (60.0 mg, 0.141 mmol, 1 equiv.), (TMP)$_2$Zn·2LiCl·2MgCl$_2$ (385 µL, 0.0846 mmol) (0.22 M in THF, 0.6 equiv.), Pd(dba)$_2$ (4.1 mg, 0.0071 mmol, 5 mol%), P(*o*-furyl)$_3$ (3.3 mg, 0.0141 mmol, 10 mol%), 4-iodobenzotrifluoride (46 mg, 0.17 mmol, 1.2 equiv.), and THF (0.28 mL). The product was purified by column chromatography on silica gel [(20 mm x 50 mL, H=23 cm of SiO$_2$) gradient elution from 5 to 15 % ethyl acetate in hexane, 5 % increases, 100 mL runs] to give **21i** (57.0 mg, 0.100 mmol, 71 % yield) as a colorless oil. **^{1}H NMR (250 MHz, CDCl$_3$)** δ 8.1 (d, J = 8.1 Hz, 2H), 7.8 (d, J = 16.1 Hz, 1H), 7.6 – 7.5 (m, 2H), 7.5 (dd, J = 7.7, 1.7 Hz, 1H), 7.3 (ddd, J = 8.3, 7.4, 1.7 Hz, 1H), 7.0 (td, J = 7.4, 1.0 Hz, 1H), 6.8 (dd, J = 8.4, 1.1 Hz, 1H), 6.3 (d, J = 16.1 Hz, 1H), 4.1 (t, J = 5.8 Hz, 2H), 4.1 (t, J = 5.8 Hz, 2H), 2.2 (quint, J = 5.8 Hz, 2H), 1.5 (s, 9H). **^{13}C NMR (63 MHz, CDCl$_3$)** δ 166.7, 160.0, 158.0, 157.0, 153.8, 147.1, 138.3, 136.9, 133.0 (q, J = 32.8 Hz), 131.4, 129.9, 128.5, 125.7 (q, J = 3.7 Hz), 123.7, 123.7 (d, J = 272.7 Hz), 121.2, 120.5, 111.8, 80.4, 71.0, 63.9, 29.8, 28.3. **^{19}F NMR (235 MHz, CDCl$_3$)** δ -63.00. **ν$_{max}$ (cm^{-1}, thin film, ATR)**: 1704, 1631, 1599, 1527, 1491, 1457, 1402, 1368, 1343, 1323, 1246, 1151, 1130, 1111, 1065, 1019, 986, 878, 855, 823, 796, 753. **HRMS (ESI+/TOF) m/z:** calc. for $[C_{27}H_{25}Cl_2F_3N_2O_4+H]^+$ 569.12162, found 569.12160.

tert-Butyl (E)-3-(2-(3-((2,4-dichloro-6-(2-methoxyphenyl)pyrimidin-5-yl)oxy)propoxy)phenyl)acrylate (21j). Pyrimidine **21j** was prepared according to **General procedure E**, using **19** (100 mg, 0.235 mmol, 1 equiv.), (TMP)$_2$Zn·2LiCl·2MgCl$_2$ (705 µL, 0.141 mmol) (0.20 M in THF, 0.6 equiv.), Pd(dba)$_2$ (6.8 mg, 0.012 mmol, 5 mol%), P(*o*-furyl)$_3$ (5.6 mg, 0.0235 mmol, 10 mol%), 2-iodoanisole (34 µL, 0.28 mmol, 1.2 equiv.), and THF (0.47 mL). Purification using Biotage [(Biotage® SNAP KP-Sil 10 g)*,* gradient elution from 10 to 20 % ethyl acetate

in hexane], gave **21j** (97.0 mg, 0.235 mmol, 78 % yield) as a yellow oil. **^{1}H NMR (250 MHz, CDCl$_3$)** δ 7.77 (d, *J* = 16.1 Hz, 1H), 7.50 (dd, *J* = 7.7, 1.7 Hz, 1H), 7.35 – 7.21 (m, 3H), 7.01 – 6.88 (m, 2H), 6.82 (d, *J* = 8.2 Hz, 1H), 6.72 (d, *J* = 8.2 Hz, 1H), 6.34 (d, *J* = 16.1 Hz, 1H), 3.93 (t, *J* = 5.7 Hz, 2H), 3.88 (t, *J* = 6.3 Hz, 2H), 3.73 (s, 3H), 2.09 – 1.96 (m, 2H), 1.51 (s, 9H). **^{13}C NMR (63 MHz, CDCl$_3$)** δ 166.8, 162.6, 157.3, 156.9, 156.0, 153.0, 147.9, 138.7, 131.9, 131.2, 130.2, 128.4, 123.7, 123.4, 120.9, 120.8, 120.3, 112.0, 111.3, 80.3, 70.5, 64.1, 55.8, 29.8, 28.3. **ν_{max} (cm^{-1}, thin film, ATR)**: 1703, 1630, 1602, 1537, 1518, 1493, 1457, 1403, 1368, 1339, 1245, 1150, 1108, 1126, 1045, 1025, 986, 952, 912, 877, 828, 753, 732. **HRMS (ESI+/TOF) m/z:** calc. for [C$_{27}$H$_{28}$Cl$_2$N$_2$O$_5$+H]$^+$ 531.14480, found 531.14490.

***tert*-Butyl (E)-3-(2-(3-((2,4-dichloro-6-(3-methoxyphenyl)pyrimidin-5-yl)oxy)propoxy)phenyl)acrylate (21k)**. Pyrimidine **21k** was prepared according to **General procedure E**, using **19** (100 mg, 0.235 mmol, 1 equiv.), (TMP)$_2$Zn·2LiCl·2MgCl$_2$ (705 µL, 0.141 mmol) (0.20 M in THF, 0.6 equiv.), Pd(dba)$_2$ (6.8 mg, 0.012 mmol, 5 mol%), P(*o*-furyl)$_3$ (5.6 mg, 0.0235 mmol, 10 mol%), 3-iodoanisole (34 µL, 0.28 mmol, 1.2 equiv.), and THF (0.47 mL). Purification using Biotage [(Biotage® SNAP KP-Sil 10 g), gradient elution from 10 to 20 % ethyl acetate in hexane], gave **21k** (94.0 mg, 0.176 mmol, 75 % yield) as a yellow oil. **^{1}H NMR (250 MHz, CDCl$_3$)** δ 7.77 (d, *J* = 16.2 Hz, 1H), 7.56 (dt, *J* = 7.7, 1.3 Hz, 1H), 7.53 – 7.46 (m, 2H), 7.37 – 7.27 (m, 1H), 7.21 (d, *J* = 7.9 Hz, 1H), 7.00 – 6.89 (m, 2H), 6.85 (d, *J* = 8.3 Hz, 1H), 6.34 (d, *J* = 16.1 Hz, 1H), 4.15 (t, *J* = 6.0 Hz, 2H), 4.01 (t, *J* = 5.7 Hz, 2H), 3.78 (s, 3H), 2.21 (quint, *J* = 5.9 Hz, 2H), 1.50 (s, 9H). **^{13}C NMR (63 MHz, CDCl$_3$)** δ 166.7, 161.7, 159.8, 157.5, 157.2, 153.6, 146.8, 138.5, 134.7, 131.3, 129.8, 128.4, 123.8, 121.7, 121.0, 120.5, 117.3, 114.5, 112.0, 80.3, 70.7, 64.2, 55.5, 29.9, 28.3. **ν_{max} (cm^{-1}, thin film, ATR)**: 1705, 1631, 1599, 1582, 1536, 1517, 1490, 1457, 1401, 1368, 1341, 1324, 1289, 1246, 1151, 1049, 986, 951, 909, 866, 783, 757, 732, 670. **HRMS (ESI+/TOF) m/z:** calc. for [C$_{27}$H$_{28}$Cl$_2$N$_2$O$_5$+H]$^+$ 531.14480, found 531.14476.

***tert*-Butyl (E)-3-(2-(3-((2,4-dichloro-6-(4-methoxyphenyl)pyrimidin-5-yl)oxy)propoxy)phenyl)acrylate (21l)**. Pyrimidine **21l** was prepared according to **General procedure E**, using **19** (85.0 mg, 0.200 mmol, 1 equiv.), (TMP)$_2$Zn·2LiCl·2MgCl$_2$ (600 µL, 0.120 mmol) (0.20 M in THF, 0.6 equiv.), Pd(dba)$_2$ (5.8 mg, 0.0100 mmol, 5 mol%), P(*o*-furyl)$_3$ (4.7 mg, 0.0200 mmol, 10 mol%), 4-

iodoanisole (30 μL, 0.24 mmol, 1.2 equiv.), and THF (0.40 mL). Purification using Biotage [(Biotage® SNAP KP-Sil 10 g), gradient elution from 10 to 20 % ethyl acetate in hexane], gave **21l** (53.0 mg, 0.100 mmol, 50 % yield) as a white solid (m.p. 107.7 – 108.2 °C). **^{1}H NMR (500 MHz, CDCl$_3$)** δ 8.1 – 8.0 (m, 2H), 7.8 (d, *J* = 16.1 Hz, 1H), 7.5 (dd, *J* = 7.7, 1.7 Hz, 1H), 7.3 (ddd, *J* = 8.6, 7.4, 1.7 Hz, 1H), 7.0 (t, *J* = 7.5 Hz, 1H), 6.9 (d, *J* = 8.1 Hz, 1H), 6.8 – 6.8 (m, 2H), 6.3 (d, *J* = 16.1 Hz, 1H), 4.2 (t, *J* = 6.0 Hz, 2H), 4.0 (t, *J* = 5.7 Hz, 2H), 3.8 (s, 3H), 2.3 (quint, *J* = 5.9 Hz, 2H), 1.5 (s, 9H). **^{13}C NMR (126 MHz, CDCl$_3$)** δ 166.8, 162.4, 161.2, 157.2, 153.6, 146.2, 138.5, 131.3, 128.5, 125.9, 123.9, 121.0, 120.6, 114.2, 112.0, 80.4, 70.2, 64.2, 55.5, 29.9, 28.3. **HRMS (ESI+/TOF) m/z:** calc. for $[C_{27}H_{28}Cl_2N_2O_5+H]^+$ 531.14480, found 531.14443.

tert-**Butyl (E)-3-(2-(3-((2,4-dichloro-6-(pyridin-4-yl)pyrimidin-5-yl)oxy)propoxy)phenyl)acrylate (21o)**. Pyrimidine **21o** was prepared according to **General procedure E**, using **19** (100 mg, 0.235 mmol, 1 equiv.), (TMP)$_2$Zn·2LiCl·2MgCl$_2$ (705 μL, 0.141 mmol) (0.20 M in THF, 0.6 equiv.), Pd(dba)$_2$ (6.8 mg, 0.012 mmol, 5 mol%), P(*o*-furyl)$_3$ (5.6 mg, 0.0235 mmol, 10 mol%), 4-iodopyridine (57.8 mg, 0.282 mmol, 1.2 equiv.), and THF (0.47 mL). Purification using Biotage [(Biotage® SNAP KP-Sil 10 g), gradient elution from 20 to 40 % ethyl acetate in hexane], gave **21o** (60.2 mg, 0.120 mmol, 51 % yield) as a brown oil. **^{1}H NMR (250 MHz, CDCl$_3$)** δ 8.6 (d, *J* = 5.2 Hz, 2H), 7.9 – 7.8 (m, 2H), 7.8 (d, *J* = 16.2 Hz, 1H), 7.5 (dd, *J* = 7.7, 1.7 Hz, 1H), 7.3 (ddd, *J* = 8.2, 7.4, 1.7 Hz, 1H), 7.0 (t, *J* = 7.4 Hz, 1H), 6.8 (d, *J* = 8.2 Hz, 1H), 6.3 (d, *J* = 16.1 Hz, 1H), 4.2 (t, *J* = 5.8 Hz, 2H), 4.1 (t, *J* = 5.9 Hz, 2H), 2.2 (quint, *J* = 5.8 Hz, 2H), 1.5 (s, 9H). **^{13}C NMR (63 MHz, CDCl$_3$)** δ 166.7, 163.7, 158.9, 158.2, 156.9, 150.3, 147.5, 141.0, 138.3, 131.4, 128.5, 123.8, 123.0, 121.3, 120.6, 111.9, 80.4, 71.4, 63.8, 29.8, 28.3. **HRMS (ESI+/TOF) m/z:** calc. for $[C_{25}H_{25}Cl_2N_3O_4+H]^+$ 502.12949, found 502.12912.

3-(2-(3-((2,4-Diaminopyrimidin-5-yl)oxy)propoxy)phenyl)propanoic acid (1). The compound was prepared according to **General procedure C**, using **21a** (100 mg, 0.234 mmol, 1 equiv.), and 4-methoxybenzylamine (306 μL, 2.34 mmol, 10 equiv.) instead of 2,4-dimethoxybenzylamine. The product was purified by column chromatography [(20 mm x 40 mL SiO$_2$), elution with 100 % ethyl acetate), affording **21a** (119 mg, 0.189 mmol, 81 % yield) as a white solid (m.p. 94.5 – 95.5 °C). **^{1}H NMR (250 MHz, CDCl$_3$)** δ 7.48 (s, 1H), 7.26 (d, *J* = 8.6 Hz, 2H), 7.16 (t, *J* = 8.4 Hz, 4H), 6.92

38

– 6.74 (m, 6H), 5.44 (s, 1H), 5.17 (s, 1H), 4.49 (t, J = 6.3 Hz, 4H), 4.16 – 4.04 (m, 5H), 3.79 (s, 7H), 2.87 (t, J = 7.7 Hz, 2H), 2.48 (dd, J = 8.5, 6.9 Hz, 2H), 2.23 (quint, J = 6.0 Hz, 2H), 1.39 (s, 8H). **^{13}C NMR (63 MHz, CDCl$_3$)** δ 172.8, 159.0, 158.7, 157.1, 156.6, 155.2, 135.2, 133.1, 132.3, 131.2, 130.1, 129.3, 129.2, 128.9, 127.6, 120.8, 114.1, 113.9, 111.2, 80.3, 66.7, 64.3, 55.4, 45.5, 43.8, 35.6, 29.5, 28.2, 26.3. **HRMS (ESI+/TOF) m/z:** calc. for $[C_{36}H_{44}N_4O_6+H]^+$ 629.33336, found 629.33343.

The above product (115 mg, 0.183 mmol, 1 equiv.) was used in the second step with anisole (201 µL, 1.83 mmol, 10 equiv.) and TFA (605 µL, 7.88 mmol, 43 equiv.) to give **1** (27 mg, 0.081 mmol, 44 % yield) as a white solid (m.p. 226.2-227.4 °C). **^{1}H NMR (250 MHz, DMSO)** δ 7.22 – 7.10 (m, 2H), 6.97 (d, J = 8.0 Hz, 1H), 6.85 (t, J = 7.3 Hz, 1H), 6.13 (s, 2H), 5.61 (s, 2H), 4.16 (t, J = 5.9 Hz, 2H), 3.79 (t, J = 5.9 Hz, 2H), 2.79 (t, J = 7.7 Hz, 2H), 2.46 (t, J = 6.6 Hz, 2H), 2.36 – 2.23 (m, 2H), 2.23 – 2.10 (m, 2H), 1.45 (quint, J = 7.4 Hz, 2H), 1.27 – 0.97 (m, 4H), 0.76 (t, J = 7.0 Hz, 3H). **^{13}C NMR (63 MHz, DMSO)** δ 174.3, 158.7, 158.3, 157.3, 156.4, 129.6, 128.8, 128.6, 127.6, 120.4, 111.3, 69.1, 64.0, 33.9, 31.2, 29.9, 29.5, 27.7, 25.5, 22.0, 14.0. **HRMS (ESI+/TOF)** m/z: calc. for [C21H30N4O4+H]+ 403.23398, found 403.23426.

3-(2-(3-((2,4-Diamino-6-pentylpyrimidin-5-yl)oxy)propoxy)phenyl)propanoic acid (3).

Pyrimidine **3** was prepared according to **General procedure C**, using **21c** (28 mg, 0.056 mmol, 1 equiv.), and 2,4-dimethoxybenzylamine (94 µL, 0.56 mmol, 10 equiv.). The product was purified by column chromatography on silica gel [(15 mm x 15 mL, H=17 cm of SiO$_2$) gradient elution from 30 to 50 % ethyl acetate in hexane, 5 % increases, 30 mL runs] to afford a pale-yellow oil (40 mg, 0.053 mmol, 94 % yield).

The above product (50.0 mg, 0.0659 mmol, 1 equiv.) was used in the second step with anisole (72 µL, 0.66 mmol, 10 equiv.) and TFA (218 µL, 2.84 mmol, 43 equiv.) to give **3** (14.0 mg, 0.0349 mmol, 53 % yield; 50 % yield for two steps) as a white solid (m.p. 183.0-184.4 °C). **^{1}H NMR (250 MHz, DMSO)** δ 7.22 – 7.10 (m, 2H), 6.97 (d, J = 8.0 Hz, 1H), 6.85 (t, J = 7.3 Hz, 1H), 6.13 (s, 2H), 5.61 (s, 2H), 4.16 (t, J = 5.9 Hz, 2H), 3.79 (t, J = 5.9 Hz, 2H), 2.79 (t, J = 7.7 Hz, 2H), 2.46 (t, J = 6.6 Hz, 2H), 2.36 – 2.23 (m, 2H), 2.23 – 2.10 (m, 2H), 1.45 (quint, J = 7.4 Hz, 2H), 1.27 – 0.97 (m, 4H), 0.76 (t, J = 7.0 Hz, 3H). **^{13}C NMR (63 MHz, DMSO)** δ 174.3, 158.7, 158.3, 157.3, 156.4, 129.6,

128.8, 128.6, 127.6, 120.4, 111.3, 69.1, 64.0, 33.9, 31.2, 29.9, 29.5, 27.7, 25.5, 22.0, 14.0. **HRMS (ESI+/TOF) m/z:** calc. for $[C_{21}H_{30}N_4O_4+H]^+$ 403.23398, found 403.23426.

3-(2-(3-((2,4-Diamino-6-(2-(trifluoromethyl)phenyl)pyrimidin-5-yl)oxy)propoxy)phenyl)propanoic acid (10). Pyrimidine **21g** (60.0 mg, 0.150 mmol, 1 equiv.) was subjected to **General procedure B**, using ethyl acetate (1 mL), and PtO_2 (5.4 mg, 0.024 mmol, 23 mol%). Purification using Biotage [(Biotage® SNAP KP-Sil 10 g), 10 % ethyl acetate in hexane] gave a colorless oil (50.0 mg, 0.0871 mmol, 83 % yield). **¹H NMR (250 MHz, CDCl₃)** δ 7.68 (d, J = 8.3 Hz, 1H), 7.56 – 7.34 (m, 3H), 7.20 – 7.05 (m, 2H), 6.87 (t, J = 7.4 Hz, 1H), 6.61 (d, J = 8.0 Hz, 1H), 3.93 (t, J = 5.8 Hz, 2H), 3.79 (t, J = 5.8 Hz, 2H), 2.74 (t, J = 7.8 Hz, 2H), 2.40 (dd, J = 8.8, 6.8 Hz, 2H), 1.99 (quint, J = 5.8 Hz, 2H), 1.43 – 1.36 (m, 9H). **¹³C NMR (63 MHz, CDCl₃)** δ 172.69, 162.83, 156.64, 156.40, 152.94, 147.22, 132.06 (q, J = 1.9 Hz), 131.66, 130.41, 130.28, 129.94, 129.03, 128.85 (q, J = 31.5 Hz), 127.42, 127.07 (q, J = 4.6 Hz), 123.67 (d, J = 274.0 Hz), 120.59, 110.87, 80.28, 70.93, 63.09, 35.44, 29.88, 28.20, 26.11. **¹⁹F NMR (235 MHz, CDCl₃)** δ -57.7. **ν$_{max}$ (cm⁻¹, thin film, ATR)**: 2963, 1726, 1523, 1495, 1455, 1403, 1370, 1340, 1315, 1245, 1171, 1144, 1117, 1051, 1036, 984, 951, 880, 801, 770, 754. **HRMS (ESI+/TOF) m/z:** calc. for $[C_{27}H_{27}Cl_2F_3N_2O_4+H]^+$ 571.13727, found 571.13719.

The above product (48.0 mg, 0.0840 mmol, 1 equiv.) was used in **General procedure C**, with 2,4-dimethoxybenzylamine (126 μL, 0.840 mmol, 10 equiv.). Purification using Biotage [(Biotage® SNAP KP-Sil 10 g), gradient elution from 30 to 50 % ethyl acetate in hexane], gave 58.0 mg (0.0697 mmol, 83 % yield) of a yellow oil. **HRMS (ESI+/TOF) m/z:** calc. for $[C_{45}H_{51}F_3N_4O_8+H]^+$ 833.37318, found 833.37293. The material (58.0 mg, 0.0697 mmol, 1 equiv.) was subjected to the following step using anisole (76 μL, 0.69 mmol, 10 equiv.) and TFA (230 μL, 3.00 mmol, 43 equiv.) to give **10** (16.0 mg, 0.0334 mmol, 48 % yield; 40 % yield for two steps) as a white solid (m.p. 180-181 °C). **¹H NMR (250 MHz, DMSO)** δ 12.0 (s, 1H), 7.7 (d, J = 7.9 Hz, 1H), 7.6 (t, J = 7.5 Hz, 1H), 7.4 (t, J = 6.5 Hz, 2H), 7.2 – 7.1 (m, 2H), 6.8 (t, J = 7.4 Hz, 1H), 6.6 (d, J = 8.1 Hz, 1H), 6.5 (s, 2H), 5.8 (s, 2H), 3.5 (t, J = 6.1 Hz, 4H), 2.6 (t, J = 7.6 Hz, 2H), 2.4 (t, J = 7.6 Hz, 2H), 1.8 (t, J = 6.2 Hz, 2H). **¹³C NMR (126 MHz, DMSO)** δ 174.0, 158.8, 156.1, 131.6, 130.8, 129.3, 128.6, 128.6, 128.6 (d, J = 87.1 Hz), 128.5, 127.3, 127.0 (q, J = 30.2 Hz), 126.0 (q, J = 4.3 Hz), 124.0 (d, J = 274.1

Hz), 120.1, 111.1, 68.8, 63.9, 33.5, 29.1, 25.2. **^{19}F NMR (235 MHz, DMSO)** δ -57.1. **HRMS (ESI+/TOF) m/z:** calc. for $[C_{23}H_{23}F_3N_4O_4+H]^+$ 477.17442, found 477.17442.

tert-**Butyl 3-(2-(3-((2,4-dichloro-6-(3-(trifluoromethyl)phenyl)pyrimidin-5-yl)oxy)propoxy)phenyl)propanoate (11)**. Pyrimidine **21h** (55.0 mg, 0.0966 mmol, 1 equiv.) was subjected to **General procedure B**, using ethyl acetate (1 mL), and PtO_2 (5.0 mg, 0.022 mmol, 23 mol%). The reaction was stirred for 6h, and the product was purified by column chromatography on silica gel [(15 mm x 17 mL, H=18 cm of SiO_2) 5 % ethyl acetate in hexane] to give a colorless oil (39.0 mg, 0.0686 mmol, 71 % yield). **^{1}H NMR (250 MHz, CDCl$_3$)** δ 8.4 (tt, *J* = 1.9, 0.8 Hz, 1H), 8.2 (dt, *J* = 7.9, 1.6 Hz, 1H), 7.7 (d, *J* = 8.2 Hz, 1H), 7.4 (t, *J* = 7.8 Hz, 1H), 7.2 – 7.1 (m, 2H), 6.9 (td, *J* = 7.4, 1.1 Hz, 1H), 6.8 (d, *J* = 8.2 Hz, 1H), 4.1 (t, *J* = 5.8 Hz, 2H), 4.0 (t, *J* = 6.0 Hz, 2H), 2.7 (dd, *J* = 8.8, 6.8 Hz, 2H), 2.4 – 2.3 (m, 2H), 2.2 (quint, J = 5.9 Hz, 2H), 1.4 (s, 9H). **^{13}C NMR (63 MHz, CDCl$_3$)** δ 172.6, 159.9, 158.0, 156.4, 153.9, 147.1, 134.3, 132.7 (d, *J* = 1.4 Hz), 131.3 (q, *J* = 32.8 Hz), 130.0, 129.4, 129.1, 128.0 (q, *J* = 3.6 Hz), 127.6, 126.5 (q, *J* = 3.9 Hz), 123.8 (d, *J* = 272.6 Hz), 120.8, 110.8, 80.2, 71.3, 63.3, 35.4, 30.0, 28.2, 26.1. **^{19}F NMR (235 MHz, CDCl$_3$)** δ -62.69. **ν_{max} (cm^{-1}, thin film, ATR)**: 2976, 1727, 1537, 1522, 1495, 1456, 1401, 1367, 1342, 1323, 1283, 1244, 1169, 1130, 1104, 1075, 1052, 983, 949, 892, 849, 791, 753, 699, 667. **HRMS (ESI+/TOF) m/z:** calc. for $[C_{27}H_{27}Cl_2F_3N_2O_4+H]^+$ 571.13727, found 571.13727.

The above product (36.0 mg, 0.0630 mmol, 1 equiv.) was used in **General procedure C**, with 2,4-dimethoxybenzylamine (95 µL, 0.630 mmol, 10 equiv.). Purification using Biotage [(Biotage® SNAP KP-Sil 10 g), gradient elution from 5 to 20 % ethyl acetate in hexane], gave 44.0 mg (0.0529 mmol, 84 % yield) of a yellow oil **HRMS (ESI+/TOF) m/z:** calc. for $[C_{45}H_{51}F_3N_4O_8+H]^+$ 833.37318, found 833.37324. The material (43.0 mg, 0.0516 mmol, 1 equiv.) was subjected to the next step using anisole (57 µL, 0.52 mmol, 10 equiv.), and TFA (171 µL, 2.23 mmol, 43 equiv.) to give **11** (18.0 mg, 0.0377 mmol, 73 % yield; 61 % yield for two steps) as a white solid (decomp. at 189 ℃). **^{1}H NMR (250 MHz, DMSO)** δ 11.95 (s, 1H), 8.19 – 8.07 (m, 2H), 7.61 (d, *J* = 7.8 Hz, 1H), 7.43 (t, *J* = 8.0 Hz, 1H), 7.21 – 7.04 (m, 2H), 6.91 – 6.78 (m, 2H), 6.65 (s, 2H), 6.00 (s, 2H), 3.94 (t, *J* = 6.2 Hz, 2H), 3.62 (t, *J* = 6.1 Hz, 2H), 2.57 (t, *J* = 7.6 Hz, 2H), 2.28 (t, *J* = 6.3 Hz, 2H), 2.03 (t, *J* = 6.2 Hz, 2H). **^{13}C NMR (151 MHz, DMSO)** δ 173.9, 159.8, 156.1, 132.3, 129.4, 129.1, 129.0, 128.8 (q, *J* = 31.5 Hz),

41

128.6, 128.2, 127.3, 125.2 (d, J = 4.2 Hz), 124.8 (d, J = 3.8 Hz), 124.2 (q, J = 272.0 Hz), 120.1, 111.2, 69.2, 64.0, 33.4, 29.2, 25.2. **^{19}F NMR (235 MHz, CDCl$_3$)** δ -61.15. **HRMS (ESI+/TOF) m/z:** calc. for $[C_{23}H_{23}F_3N_4O_4+H]^+$ 477.17442, found 477.17498.

3-(2-(3-((2,4-Diamino-6-(4-(trifluoromethyl)phenyl)pyrimidin-5-yl)oxy)propoxy)phenyl)propanoic acid (12). Pyrimidine **21i** (55.0 mg, 0.0966 mmol, 1 equiv.) was subjected to **General procedure B**, using ethyl acetate (1 mL), and PtO$_2$ (5.0 mg, 0.022 mmol, 23 mol%). The reaction was stirred for 6h, and the product was purified by column chromatography on silica gel [(15 mm x 17 mL, H=18 cm of SiO$_2$) 5 % ethyl acetate in hexane] to give a colorless oil (45.0 mg, 0.0792 mmol, 82 % yield). **^{1}H NMR (250 MHz, CDCl$_3$)** δ 8.1 (d, J = 8.2 Hz, 2H), 7.6 (d, J = 8.3 Hz, 2H), 7.2 – 7.1 (m, 2H), 6.9 (td, J = 7.4, 1.1 Hz, 1H), 6.8 (d, J = 8.0 Hz, 1H), 4.2 – 4.0 (m, 4H), 2.7 (dd, J = 8.8, 6.8 Hz, 2H), 2.3 (dd, J = 8.7, 6.9 Hz, 2H), 2.2 (quint, J = 5.9 Hz, 2H), 1.4 (s, 9H). **^{13}C NMR (63 MHz, CDCl$_3$)** δ 172.6, 160.0, 158.1, 156.4, 153.8, 147.2, 136.9 (d, J = 1.4 Hz), 133.0 (q, J = 32.8 Hz), 130.2, 129.9, 129.0, 127.6, 125.7 (q, J = 3.8 Hz), 123.7 (d, J = 272.8 Hz), 120.9, 110.7, 80.2, 71.3, 63.2, 35.4, 30.0, 26.1. **^{19}F NMR (235 MHz, CDCl$_3$)** δ -62.98. **ν_{max} (cm^{-1}, thin film, ATR)**: 2972, 1727, 1527, 1496, 1401, 1367, 1342, 1323, 1244, 1171, 1131, 1113, 1065, 1019, 984, 948, 881, 855, 796, 753. **HRMS (ESI+/TOF) m/z:** calc. for $[C_{27}H_{27}Cl_2F_3N_2O_4+H]^+$ 571.13727, found 571.13741.

The above product (42.0 mg, 0.0735 mmol, 1 equiv.) was used in **General procedure C**, with 2,4-dimethoxybenzylamine (110 μL, 0.735 mmol, 10 equiv.). Purification using Biotage [(Biotage® SNAP KP-Sil 10 g), gradient elution from 5 to 20 % ethyl acetate in hexane], gave 49.0 mg (0.0588 mmol, 80 % yield) of a yellow oil **HRMS (ESI+/TOF) m/z:** calc. for $[C_{45}H_{51}F_3N_4O_8+H]^+$ 833.37318, found 833.37327. The product (49.0 mg, 0.0588 mmol, 1 equiv.) was subjected to the next step using anisole (65 μL, 0.59 mmol, 10 equiv.) and TFA (195 μL, 2.54 mmol, 43 equiv.) to give **12** (20.0 mg, 0.0417 mmol, 71 % yield; 57 % yield for two steps) as a white solid (m.p. 214-216 °C). **^{1}H NMR (250 MHz, DMSO)** δ 11.96 (s, 1H), 8.04 (d, J = 8.1 Hz, 2H), 7.56 (d, J = 8.3 Hz, 2H), 7.22 – 7.03 (m, 2H), 6.92 – 6.78 (m, 2H), 6.49 (s, 2H), 5.84 (s, 2H), 3.96 (t, J = 6.0 Hz, 2H), 3.62 (t, J = 6.1 Hz, 2H), 2.58 (t, J = 7.6 Hz, 2H), 2.25 (dd, J = 8.2, 7.0 Hz, 2H), 2.14 – 1.98 (m, 2H). **^{13}C NMR (126 MHz, DMSO)** δ 173.9, 159.7, 159.2, 156.1, 151.2, 140.7, 129.4, 129.2, 129.1, 128.7 (d, J = 31.7 Hz), 128.5, 127.3, 124.6

(q, *J* = 3.9 Hz), 124.1 (d, *J* = 272.2 Hz), 120.1, 111.0, 68.9, 63.9, 33.4, 29.2, 25.2. **¹⁹F NMR (235 MHz, CDCl₃)** δ -61.08. **HRMS (ESI+/TOF) m/z:** calc. for $[C_{23}H_{23}F_3N_4O_4]^+$ 477.17442, found 477.17422.

3-(2-(3-((2,4-Diamino-6-(2-methoxyphenyl)pyrimidin-5-yl)oxy)propoxy)phenyl)propanoic acid (13). Pyrimidine **21j** (95.0 mg, 0.179 mmol, 1 equiv.) was subjected to **General procedure B**, using ethyl acetate (1.8 mL), and PtO₂ (9.3 mg, 0.041 mmol, 23 mol%). After 4 h, another portion of PtO₂ (9 mg) was added, and the reaction was stirred for another 4 h. Purification using Biotage [(Biotage® SNAP KP-Sil 10 g), gradient elution from 10 to 20 % ethyl acetate in hexane], gave a colorless oil (88.0 mg, 0.165 mmol, 92 % yield). **¹H NMR (250 MHz, CDCl₃)** δ 7.4 – 7.3 (m, 2H), 7.2 – 7.1 (m, 2H), 7.0 (td, *J* = 7.5, 1.0 Hz, 1H), 6.9 – 6.8 (m, 2H), 6.7 – 6.6 (m, 1H), 3.9 (t, *J* = 5.8 Hz, 2H), 3.8 (t, *J* = 6.0 Hz, 2H), 3.8 (s, 3H), 2.8 (dd, *J* = 8.7, 6.8 Hz, 2H), 2.4 – 2.4 (m, 2H), 2.0 (quint, J = 5.9 Hz, 2H), 1.4 (s, 9H). **¹³C NMR (63 MHz, CDCl₃)** δ 172.7, 162.5, 157.0, 156.5, 156.0, 152.9, 148.0, 131.9, 130.3, 130.0, 129.1, 127.4, 123.6, 120.8, 120.6, 111.4, 111.0, 80.2, 70.9, 63.5, 55.8, 35.4, 30.0, 28.2, 26.2. **ν_max (cm⁻¹, thin film, ATR)**: 2976, 1727, 1603, 1584, 1537, 1518, 1495, 1456, 1402, 1367, 1339, 1286, 1243, 1148, 1113, 1086, 1046, 1025, 984, 951, 879, 828, 753. **HRMS (ESI+/TOF) m/z:** calc. for $[C_{27}H_{30}Cl_2N_2O_5+H]^+$ 533.16045, found 533.16086.

The above product (85.0 mg, 0.159 mmol, 1 equiv.) was used in **General procedure C**, with 2,4-dimethoxybenzylamine (239 µL, 1.59 mmol, 10 equiv.). Purification using Biotage [(Biotage® SNAP KP-Sil 10 g), gradient elution from 30 to 50 % ethyl acetate in hexane], gave 95.0 mg (0.119 mmol, 75 % yield) of a white solid. **HRMS (ESI+/TOF) m/z:** calc. for $[C_{45}H_{54}N_4O_9+H]^+$ 795.39636, found 795.39548. The material (93.0 mg, 0.117 mmol, 1 equiv.) was subjected to the next step using anisole (128 µL, 1.17 mmol, 10 equiv.) and TFA (387 µL, 5.04 mmol, 43 equiv.) to give **13** (22.0 mg, 0.0503 mmol, 43 % yield; 32 % yield for two steps) as a white solid (decomp. at 120°C). **¹H NMR (300 MHz, DMSO)** δ 12.04 (s, 1H), 7.26 (ddd, *J* = 8.3, 7.4, 1.8 Hz, 1H), 7.22 – 7.05 (m, 3H), 6.97 (d, *J* = 8.1 Hz, 1H), 6.90 (td, *J* = 7.4, 1.0 Hz, 1H), 6.82 (td, *J* = 7.4, 1.1 Hz, 1H), 6.67 (d, *J* = 8.1 Hz, 1H), 6.26 (s, 2H), 5.67 (s, 2H), 3.69 (s, 3H), 3.61 – 3.50 (m, 4H), 2.66 (t, *J* = 7.6 Hz, 2H), 2.39 (dd, *J* = 8.3, 6.9 Hz, 2H), 1.79 (quint, J = 6.3 Hz, 2H). **¹³C NMR (75 MHz, DMSO)** δ 174.0, 158.8,

43

158.6, 156.4, 156.2, 154.3, 129.8, 129.3, 129.3, 128.5, 127.3, 126.7, 120.0, 119.7, 111.2, 111.0, 68.8, 64.3, 55.2, 33.5, 29.2, 25.3. **HRMS (ESI+/TOF) m/z:** calc. for $[C_{23}H_{26}N_4O_5+H]^+$ 439.19760, found 439.19798.

3-(2-(3-((2,4-Diamino-6-(3-methoxyphenyl)pyrimidin-5-yl)oxy)propoxy)phenyl)propanoic acid (14).

Pyrimidine **21k** (92.0 mg, 0.173 mmol, 1 equiv.) was subjected to **General procedure B**, using ethyl acetate (1.7 mL), and PtO$_2$ (9.0 mg, 0.039 mmol, 23 mol%). After 4h, another portion of PtO$_2$ (9 mg) was added, and the reaction was stirred for another 4h. Purification using Biotage [(Biotage® SNAP KP-Sil 10 g), gradient elution from 10 to 20 % ethyl acetate in hexane], gave a colorless oil (88.0 mg, 0.152 mmol, 88 % yield). **¹H NMR (250 MHz, CDCl₃)** δ 7.6 – 7.5 (m, 2H), 7.3 – 7.2 (m, 1H), 7.2 (ddd, *J* = 16.0, 7.9, 1.7 Hz, 2H), 7.0 (ddd, *J* = 8.3, 2.7, 1.0 Hz, 1H), 6.9 (td, *J* = 7.4, 1.1 Hz, 1H), 6.8 (dd, *J* = 8.1, 1.1 Hz, 1H), 4.1 (t, *J* = 6.0 Hz, 2H), 4.0 (t, *J* = 5.9 Hz, 2H), 3.8 (s, 3H), 2.8 (dd, *J* = 8.7, 6.8 Hz, 2H), 2.4 (dd, *J* = 8.6, 6.9 Hz, 2H), 2.2 (quint, J = 5.9 Hz, 2H), 1.4 (s, 9H). **¹³C NMR (63 MHz, CDCl₃)** δ 172.7, 161.6, 159.8, 157.6, 156.5, 153.6, 146.9, 134.8, 130.0, 129.8, 129.2, 127.5, 121.8, 120.6, 117.4, 114.6, 110.9, 80.2, 71.0, 63.5, 55.5, 35.4, 30.1, 28.2, 26.2. **ν$_{max}$ (cm⁻¹, thin film, ATR)**: 2974, 1728, 1601, 1584, 1537, 1517, 1494, 1455, 1400, 1368, 1340, 1288, 1243, 1148, 1113, 1049, 983, 950, 907, 861, 782, 756, 698, 670. **HRMS (ESI+/TOF) m/z:** calc. for $[C_{27}H_{30}Cl_2N_2O_5+H]^+$ 533.16045, found 533.16018.

The above product (77.0 mg, 0.144 mmol, 1 equiv.) was used in **General procedure C**, with 2,4-dimethoxybenzylamine (217 µL, 1.44 mmol, 10 equiv.). Purification using Biotage [(Biotage® SNAP KP-Sil 10 g), gradient elution from 10 to 30 % ethyl acetate in hexane], gave 86.0 mg (0.108 mmol, 75 % yield) of a yellow oil **HRMS (ESI+/TOF) m/z:** calc. for $[C_{45}H_{54}N_4O_9+H]^+$ 795.39636, found 795.39600. The material (85.0 mg, 0.107 mmol, 1 equiv.) was subjected to the next step using anisole (117 µL, 1.07 mmol, 10 equiv.), and TFA (354 µL, 4.61 mmol, 43 equiv.) to give **14** (28.0 mg, 0.0642 mmol, 60 % yield; 45 % yield for two steps) as a white solid (m.p. 148.0-149.0 °C). **¹H NMR (300 MHz, DMSO)** δ 12.00 (s, 1H), 7.45 – 7.34 (m, 2H), 7.17 (td, *J* = 7.7, 1.5 Hz, 2H), 7.10 (dd, *J* = 7.4, 1.7 Hz, 1H), 6.89 – 6.79 (m, 3H), 6.34 (s, 2H), 5.74 (s, 2H), 3.94 (t, *J* = 6.3 Hz, 2H), 3.72 (s, 3H), 3.59 (t, *J* = 6.1 Hz, 2H), 2.63 (t, *J* = 7.6 Hz, 2H), 2.34 (t, *J* = 7.6 Hz, 2H), 2.02 (quint, J = 6.2 Hz, 2H). **¹³C NMR**

(75 MHz, DMSO) δ 174.0, 159.6, 159.0, 158.7, 156.2, 152.7, 138.1, 129.3, 128.8, 128.8, 128.6, 127.3, 120.8, 120.1, 114.1, 113.8, 111.2, 68.8, 64.3, 54.9, 33.4, 29.3, 25.2. **HRMS (ESI+/TOF) m/z:** calc. for $[C_{23}H_{26}N_4O_5+H]^+$ 439.19760, found 439.19806.

3-(2-(3-((2,4-Diamino-6-(4-methoxyphenyl)pyrimidin-5-yl)oxy)propoxy)phenyl)propanoic acid (15). Pyrimidine **21l** (84.0 mg, 0.158 mmol, 1 equiv.) was subjected to **General procedure B**, using ethyl acetate (1.6 mL), and PtO$_2$ (8.2 mg, 0.036 mmol, 23 mol%). The reaction mixture was stirred for 6h. Purification using Biotage [(Biotage® SNAP KP-Sil 10 g), gradient elution from 10 to 15 % ethyl acetate in hexane], gave **34.6.2** (72.0 mg, 0.134 mmol, 85 % yield) a colorless oil. **¹H NMR (500 MHz, CDCl₃)** δ 8.1 – 8.1 (m, 2H), 7.2 (td, *J* = 7.8, 1.7 Hz, 1H), 7.1 (dd, *J* = 7.4, 1.7 Hz, 1H), 6.9 (td, *J* = 7.4, 1.1 Hz, 1H), 6.8 – 6.8 (m, 3H), 4.1 (t, *J* = 5.8 Hz, 2H), 4.0 (t, *J* = 5.8 Hz, 2H), 3.8 (s, 3H), 2.7 (dd, *J* = 8.9, 6.7 Hz, 2H), 2.4 – 2.3 (m, 2H), 2.2 (quint, J = 5.9 Hz, 2H), 1.4 (s, 9H). **¹³C NMR (126 MHz, CDCl₃)** δ 172.7, 162.4, 161.1, 157.3, 156.5, 153.6, 146.2, 131.4, 130.1, 129.2, 127.6, 125.9, 120.7, 114.2, 110.8, 80.2, 70.4, 63.4, 55.5, 35.4, 30.1, 28.2, 26.2. **HRMS (ESI+/TOF) m/z:** calc. for $[C_{27}H_{30}Cl_2N_2O_5+H]^+$ 533.16045, found 533.16035.

The above product (72.0 mg, 0.135 mmol, 1 equiv.) was used in **General procedure C**, with 2,4-dimethoxybenzylamine (203 µL, 1.35 mmol, 10 equiv.). Purification using Biotage [(Biotage® SNAP KP-Sil 10 g), gradient elution from 10 to 30 % ethyl acetate in hexane], gave 89.0 mg (0.112 mmol, 83 % yield) of a colorless oil **HRMS (ESI+/TOF) m/z:** calc. for $[C_{45}H_{54}N_4O_9+H]^+$ 795.39636, found 795.39589. The product of the previous reaction (89.0 mg, 0.112 mmol, 1 equiv.) was subjected to the next step using anisole (123 µL, 1.12 mmol, 10 equiv.) and TFA (370 µL, 4.83 mmol, 43 equiv.) to give **15** (26.0 mg, 0.0594 mmol, 53 % yield; 44 % yield for two steps) as a white solid (m.p. 222.5-223.9 °C). **¹H NMR (300 MHz, DMSO)** δ 11.99 (s, 1H), 7.92 – 7.79 (m, 2H), 7.22 – 7.07 (m, 2H), 6.94 – 6.81 (m, 2H), 6.81 – 6.74 (m, 2H), 6.26 (s, 2H), 5.67 (s, 2H), 3.99 (t, *J* = 6.1 Hz, 2H), 3.65 (s, 3H), 3.62 (t, *J* = 6.1 Hz, 2H), 2.62 (t, *J* = 7.6 Hz, 2H), 2.30 (dd, *J* = 8.2, 7.0 Hz, 2H), 2.06 (quint, J = 6.1 Hz, 2H). **¹³C NMR (75 MHz, DMSO)** δ 174.0, 159.5, 159.5, 159.0, 156.2, 152.3, 129.8, 129.4, 129.0, 128.6, 128.4, 127.4, 120.1, 113.0, 111.1, 68.3, 64.1, 54.9, 33.4, 29.3, 25.3. **HRMS (ESI+/TOF) m/z:** calc. for $[C_{23}H_{26}N_4O_5+H]^+$ 439.19760, found 439.19792.

3-(2-(3-((2,4-Diamino-6-(pyridin-4-yl)pyrimidin-5-yl)oxy)propoxy)phenyl)propanoic acid (18). Pyrimidine **21o** (123 mg, 0.245 mmol, 1 equiv.) was subjected to **General procedure B**, using ethyl acetate (2.5 mL), and PtO$_2$ (12.7 mg, 0.0558 mmol, 23 mol%). After 4h, another portion of PtO$_2$ was added (12 mg), and the mixture was stirred for another 4h. Purification using Biotage [(Biotage® SNAP KP-Sil 10 g), gradient elution from 20 to 40 % ethyl acetate in hexane], gave a yellow oil (58.2 mg, 0.115 mmol, 47 % yield). **¹H NMR (250 MHz, CDCl$_3$)** δ 8.68 – 8.60 (m, 2H), 7.95 – 7.88 (m, 2H), 7.26 – 7.11 (m, 2H), 6.92 (td, *J* = 7.4, 1.1 Hz, 1H), 6.80 (dd, *J* = 8.1, 1.1 Hz, 1H), 4.20 – 4.04 (m, 4H), 2.75 (t, *J* = 8.1, 7.6 Hz, 2H), 2.46 – 2.33 (m, 2H), 2.24 (quint, J = 5.8 Hz, 2H), 1.40 (s, 9H). **¹³C NMR (63 MHz, CDCl$_3$)** δ 172.6, 158.8, 158.2, 156.3, 154.0, 150.4, 147.6, 141.0, 130.1, 129.1, 127.6, 123.1, 120.9, 110.7, 80.2, 71.6, 63.2, 35.4, 30.0, 28.2, 26.1. **ν$_{max}$ (cm⁻¹, thin film, ATR)**: 2979, 1726, 1599, 1535, 1519, 1494, 1455, 1403, 1367, 1346, 1317, 1244, 1176, 1148, 1113, 1051, 983, 949, 882, 844, 818, 788, 753, 631. **HRMS (ESI+/TOF) m/z:** calc. for [C$_{25}$H$_{27}$Cl$_2$N$_3$O$_4$+H]$^+$ 504.14514, found 504.14524.

The above product (57.0 mg, 0.113 mmol, 1 equiv.) was used in **General procedure C**, with 2,4-dimethoxybenzylamine (170 µL, 1.13 mmol, 10 equiv.). Purification using Biotage [(Biotage® SNAP KP-Sil 10 g), gradient elution from 60 to 100 % ethyl acetate in hexane], gave 66.8 mg (0.0870 mmol, 77 % yield) of a colorless oil. **HRMS (ESI+/TOF) m/z:** calc. for [C$_{43}$H$_{51}$N$_5$O$_8$+H]$^+$ 766.38104, found 766.38009. The material (66.0 mg, 0.0862 mmol, 1 equiv.) was subjected to the next step using anisole (95 µL, 0.86 mmol, 10 equiv.) and TFA (285 µL, 3.71 mmol, 43 equiv.). In this case, the reaction mixture was heated at 70 °C for 48 h to fully deprotect the DMB groups, affording **18** (16.1 mg, 0.0388 mmol, 45 % yield; 35 % yield for two steps) as a white solid (m.p. 240.2 – 241.7 °C). **¹H NMR (250 MHz, DMSO)** δ 11.99 (s, 1H), 8.44 (d, *J* = 5.1 Hz, 2H), 7.76 (d, *J* = 5.8 Hz, 2H), 7.25 – 7.05 (m, 2H), 6.95 – 6.79 (m, 2H), 6.53 (s, 2H), 5.88 (s, 2H), 3.99 (t, *J* = 6.1 Hz, 2H), 3.63 (t, *J* = 6.1 Hz, 2H), 2.61 (t, *J* = 7.6 Hz, 2H), 2.30 (t, *J* = 7.6 Hz, 2H), 2.06 (quint, J = 6.9, 6.1, 6.1, 5.4 Hz, 2H). **¹³C NMR (126 MHz, DMSO)** δ 173.9, 159.7, 159.2, 156.1, 149.5, 129.6, 129.4, 128.6, 127.4, 122.6, 120.2, 111.2, 69.2, 64.0, 33.4, 29.2, 25.2. **HRMS (ESI+/TOF) m/z:** calc. for [C$_{21}$H$_{23}$N$_5$O$_4$+H]$^+$ 410.18228, found 410.18263.

MulDHFR Protein Production, Crystallization and Structure Determination. Cloning, expression and purification were conducted as part of the Seattle Structural Genomics Center for Infectious Disease (SSGCID) following standard protocols described previously.[34,51–55] Prokaryotic expression vectors containing the cysteine-89 variant mutant (C89S) of *M. ulcerans* DHFR were obtained from the Seattle Structural Genomics Center for Infectious Disease (clone ID MyulA.01062.a.B11.GE42658, respectively; www.SSGCID.org). The C89S variant was created by performing site-directed mutagenesis on the WT using a Quick-Change Lightning kit, based upon the UCLA MBI-SERp Server Identification of high surface-entropy residues. Primers were designed using the Quick-Change Primer Design Program available online at www.agilent.com/genomics/qcpd.

The gene was cloned into the ligation independent cloning (LIC) expression vector pBG1861 encoding a non-cleavable, N-terminal 6xHis fusion tag (amino acid sequence: MAHHHHHH).[53] Plasmid DNA was transformed into chemically competent *E. coli* BL21(DE3)R3 Rosetta cells. The plasmid containing MulDHFR-C89S was expression tested and 2 litres of culture were grown using auto-induction media[56] in a LEX Bioreactor (Epiphyte Three Inc.) as previously described.[57]

MulDHFR-C89S was purified in a two-step protocol consisting of a Ni^{2+}-affinity chromatography (IMAC) step and size-exclusion chromatography (SEC). All chromatography runs were performed on an ÄKTApurifier 10 (GE) using automated IMAC and SEC programs according to previously described procedures.[55] Bacterial pellets-thawed in a 42 °C water bath and vortexed gently were resuspended in 180 ml lysis buffer containing 20 mM HEPES pH 7.2–7.4, 300 mM NaCl, 5 % (v/v) glycerol, 0.5 % CHAPS, 30 mM imidazole, 21 mM $MgCl_2$, 1 mM TCEP, and 2 protease inhibitor tablets and lysed by sonication for 15 minutes (5 s on, 10 s off, 70 % amplitude, on ice). After sonication, the crude lysate was clarified with 2 µl of benzonase and incubated while mixing at room temperature for 45 minutes. The lysate was then clarified by centrifugation at 10 000 rev min^{-1} for 1 h at 4 °C using a Sorvall centrifuge (Thermo Scientific). The supernatant was filtered through a 0.45 µM syringe filter, then passed over a Ni-NTA His-Trap FF 5 ml column (GE Healthcare) which was pre-equilibrated with loading buffer composed of 20 mM HEPES pH 7.0, 300 mM NaCl, 5 % (v/v) glycerol, and 30 mM Imidazole. The column

was washed with 20 column volumes (CV) of loading buffer and was eluted with 10 CVs of loading buffer plus 0.5 M imidazole. Peak fractions, as determined by UV at 280 nm, were pooled and concentrated to 5 ml with a 3 K Pall filter. A SEC column (Superdex 75, GE) was equilibrated with running buffer composed of 300 mM NaCl, 20 mM HEPES pH 7.0, 5 % (v/v) glycerol, and 1 mM TCEP. The peak fractions were collected and analyzed for the presence of the protein of interest using SDS-PAGE. The peak fractions were pooled and concentrated using an Amicon purification system (Millipore). Aliquots of 110 µl were flash-frozen in a dry ice and ethanol bath and stored at −80 °C until use. The protein was quantitated by UV-light (extinction coefficient of 37 470 M^{-1} cm^{-1}) using a Nanodrop spectrophotometer (Thermo). The molecular mass of the purified protein was confirmed by intact mass, LC-MS.

For crystallization, NADP and DHFR inhibitors were added to purified MulDHFR-C89S (12.5 mg.ml^{-1}) at 6-fold molar excess. Sitting drops were set at 1 : 1 ratio composed of 400 nL of the protein-inhibitor–NADP mixture to 400 nL reservoir solution. Crystallization experiments were performed at 14 °C. Additional crystallization experiments were set up using an NT8 drop setting robot (Formulatrix Inc.) and UVXPO MRC (Molecular Dimensions) sitting drop vapor diffusion plates at 18 °C. 100 nL protein and 100 nL crystallization solution were dispensed and equilibrated against 50 µL of the crystallization solution. The best-diffracting crystals grew from the Morpheus[58] (Molecular Dimensions), PACT (Molecular Dimensions) and Berkeley[59] (Rigaku Reagents) crystallization screens as noted in Additional_Data_File1. Because of the makeup of the mother liquor, crystals were vitrified in liquid nitrogen with no additional cryo-protection. Diffraction data were collected at LS-CAT at the Advanced Photon Source Life Sciences Collaborative Access Team (APS LS-CAT) beamline 21-ID-D equipped with a Dectris Eiger 9M detector at a wavelength of 0.8666 Å. Data sets were reduced with the XDS package.[60] Molecular replacement (MR) was performed with Molrep[61] from the CCP4 package,[62] using the *M. tuberculosis* structure as template (PDB ID 1DF7).[41] Manual model building was performed using Coot,[63] the structure was refined in reciprocal space with Phenix.[64] NADP and **P218** atoms were refined with full (1.0) occupancy. Structure validation was performed using MolProbity.[65]

48

MabDHFR, MavDHFR and HsaDHFR Protein Production for enzymatic assays. Full length coding DNA clones for *M. abscessus* and *M. avium* DHFRs were kind gits from the Seattle Structural Genomics Center for Infectious Disease (SSGCID) and used as template for PCR amplification. Amplicons encompassing the full-length DHFR enzymes of MavDHFR (residues Met1 to Ser176) and MabDHFR (residues Met1 to Gly163) were cloned into plasmid pNIC28-Bsa4 via ligation-independent cloning.[66] Full-length human DHFR (residues Met1 to Asp187) cloned into *E. coli* expression vector pET28 was a kind gift of the Seattle Structural Genomics Center for Infectious Disease (SSGCID).

For protein production, *E. coli* BL21(DE3)R3 Rosetta cells having the appropriate plasmids were cultivated in TB medium (supplemented with 50 µg.ml^{-1} kanamycin, 35 µg.ml^{-1} chloramphenicol) at 37 °C until OD$_{600}$ reached ~3 and then cooled to 18 °C for 1 hour. Isopropyl 1-thio-D-galactopyranoside (IPTG) was added to 0.1 mM, and growth continued at 18 °C overnight. Cells were collected by centrifugation (15 min at 7,500 × g 4 °C) and pellets suspended in 2x Binding Buffer (1 mL of 2x Binding Buffer per gram of cell pellet) complemented with 0.1 % DDM (n-Dodecyl β-D-maltoside) and Protease Inhibitors Cocktail Set VII (Calbiochem, 1/1000 dilution). 2x Binding Buffer is 50 mM Tris-HCl, pH 8.0, 0.6 M NaCl, 100 mM Arginine, 20 % (v/v) glycerol and (fresh) 1 mM (2-carboxyethyl)phosphine – TCEP. Pellets were flash-frozen in liquid nitrogen and stored at -80 °C until use.

For protein purification, 1x Binding Buffer was added (3 mL per g of cell pellet) to cell pellets and the solution mixed to homogeneity. Cells were lysed by sonication on ice (5 sec active sonication followed by a 10 sec interval for a total of 4 minutes of active sonication at 35 % amplitude). Polyethyleneimine (pH 7.5) was added to the cell lysate at a final concentration of 0.15 % (v/v) and the solution gently mixed prior to centrifugation (53,000 × g for 45 min at 4 °C). Proteins were purified using Ni-Sepharose resin (GE Healthcare) and eluted stepwise in Binding Buffer with 300 mM imidazole. Proteins were further purified by gel filtration (Superdex 200 16/60, GE Healthcare) in GF buffer - 20mM HEPES, pH 7.50, 0.3M NaCl, 5 %(v/v) glycerol, 0.5 mM TCEP (fresh). Proteins in gel filtration buffer were concentrated to 2.0 mg.ml^{-1} (measured by UV absorbance with a NanoDrop spectrophotometer - Thermo Scientific; using the calculated molecular weight and

estimated extinction coefficient) using 30 kDa MWCO centrifugal concentrators (Millipore) at 4 °C, flash frozen in a liquid nitrogen bath and stored at -80 °C until use.

Enzymatic assays. Assays were executed with purified, recombinant DHFR from *Mycobacteria abcessus* (MabDHFR), *Mycobacteria avium* (MavDHFR) and human (HsaDHFR). Their activity was assessed by reduction of dihydronicotinamide-adenine dinucleotide phosphate (NADPH) followed by transformation of dihydrofolate in tetrahydrofolate.[34] First, purified enzymes were diluted in a solution containing 50 mM PIPES pH 7.3, 0.02 % Tween-20, 400 µM NADPH, 1.5 mg/ml BSA and 6 mM DTT. Then, 20µL of this mixture was add to a 384-well, black, non-binding plates (Corning). The reaction was started by the addition of 10 µL of 7,8-dihydrofolate to a final concentration of 400 µM for MavDHFR and MabDHFR, and 133 µM for HsaDHFR.

NADPH consumption measured by fluorescence intensity was followed (excitation 340 nm/emission 445 nm) for 30 minutes at 25 °C using a ClarioSTAR® (BMG Labtech) plate reader. The slope of the linear part of each well was used to measure the enzyme activity.

To calculate compounds half-maximal inhibitory concentration (IC_{50}), 100 nL of serial diluted inhibitors were added to the reaction using an automated liquid handler robot (Felix, Analytik Jena AG) and incubated for 1 h at room temperature before the addition of 7,8-dihydrofolate. Final DMSO concentration was 0.3 %. To normalize data, the reaction rate was measured in the absence of inhibitors (DMSO only, 100 % activity), and in the absence of the enzyme (0 % activity). Inhibitory constant (K_i) was calculated assuming competitive inhibition using the Cheng-Prusoff equation. Plots and analysis were done using GraphPad Prism 9.0. Compounds were tested at least twice in duplicate or triplicate, and all values plotted together for final calculations.

Strain and culture conditions. *Mycobacterium abscessus* ATCC 19977 and *Mycobacterium avium* subsp. *hominissuis* 104 (MAH) were grown in rolling liquid culture at 37 °C in Middlebrook 7H9 (BD Difco) supplemented with 10 % (v/v) albumin-dextrose-catalase, 0.2 % (v/v) glycerol, and 0.05 % (v/v) Tween 80 (7H9 complete).

Whole-cell activity of compounds/Minimum inhibitory concentrations (MIC). MIC values were determined using the resazurin microtiter assay (REMA). Cultures were grown to log phase (OD_{600} of 0.4-0.8) and diluted to OD_{600} of 0.005. Lyophilized compounds were resuspended in dimethyl sulfoxide (DMSO) and diluted to 10 % DMSO in 7H9 complete. Compounds were prepared in two-fold serial dilutions with 7H9 complete in 96-well clear, flat bottom plates (Falcon) with 90 µL of bacteria (OD_{600} 0.005) per well to a final volume of 100 µL. Plates were incubated statically at 37 °C until drug-free wells were turbid (2 days for *M. abscessus*, 4 days for MAH 104). Ten µL of resazurin (Sigma) prepared at 0.025 % (w/v) in distilled water was added to each well. Plates were incubated for 4 hours (*M. abscessus*) or 8 hours (MAH) at 37 °C until the drug-free wells turned pink (approximately one doubling time). Fluorescence (Ex/Em 560/590) was measured using an Infinite F200 Tecan plate reader. Fluorescence intensities were converted to percentage of viable cells relative to drug-free conditions and fit to a four-parameter dose-response regression or a modified four-parameter dose-response regression using GraphPad Prism version 9. MIC values were determined from the modified four-parameter dose-response regression (Gompertz nonlinear regression).[40]

Solubility determination "RelSOL". Solubility was assessed using an "in-house" developed method known as "RelSOL". This solubility method measures the solubility in physiological strength phosphate buffered saline starting from 10 mM DMSO solutions of the test compounds. Test compounds were dissolved in DMSO to give 10 mM solutions. Solubility test samples were prepared by adding a volume (5 µL) of the 10 mM solution to a volume (195 µL) of phosphate buffered saline, pH 7.4 (Sigma-Aldrich, Cat no. P4417, made as per manufacturer's instructions). This solution was mixed for 24 hours (rotary mixing, 900 rpm, 25°C), excluding light. After mixing, the solubility test samples were filtered to remove any undissolved material using a proprietary filter (Millipore Multiscreen HTS filter, 96-well format). Samples were drawn through the filter using vacuum. The filtrate from the above was analyzed for dissolved drug compound using a truncated UHPLC methodology. A Shimadzu Nexera X2 UHPLC system was used, with a reversed-phase column and a simple formic acid gradient elution. The UHPLC parameters

are: *mobile phase component A*: HPLC water with 0.1 % formic acid; *mobile phase component B*: HPLC acetonitrile with 0.1 % formic acid; flow rate: 0.6 mL/min; gradient: Initial 2 % B in A, at 1.4 min: 98 % B, at 3.0 min 98 % B, *re-equilibration time* 1 min; *autosampler temperature*: 25 °C; *column*: Hypersil Gold, C18 1.9 µm, 50 x 2.1 mm; *column temperature*: 50 °C; *detector wavelength*: 254 nm; *bandwidth*: 4 nm. A calibration solution was prepared in the following way: The same 10 mM solution used to prepare the solubility test sample was diluted in DMSO to give a 500 µM solution. This solution was then diluted with 50:50 acetonitrile:water to provide a 50 µM solution. Aliquots (0.2, 1.0 and 5.0 µL) of this 50 µM solution were then injected into the UHPLC system, and the areas of the resultant peaks integrated to produce a calibration line. Aliquots of the test sample filtrate (0.4 and 5.0 µL) were then injected onto the UHPLC system, and the resultant peak areas for any peaks corresponding to the test compound were determined and quantified using the calibration line (the injection volume that gave a peak area closest to the calibrated range was used for determining solubility).

MDCK Passive Permeability. MDCK-II cells (Netherlands Cancer Institute) were maintained in culture (DMEM, Gibco Cat: 61965-026 supplemented with 1 % penicillin/streptomycin, 10 % Fetal Calf Serum) until required. For experimentation, cells were seeded onto individual transwell 'Thincerts' (Greiner, Cat 662610) at a density of 35,000 cells/well. Cells were grown at 37 °C, 5 % CO_2 for 3 days. On day 4, the media was replaced with fresh media and incubated for 1 hour. Media was removed and replaced with Dulbecco's Phosphate Buffered Saline (Gibco, 14287-080), and cell inserts were incubated for an additional 1 hour. Dosing solutions containing 3 µM Test Compound, 100 µM Lucifer Yellow (1 % DMSO) were prepared. 1.2 mL of Phosphate Buffered Saline (1 % DMSO) was added to wells of a 24-well cell culture plate (Corning, Cat 353504). 0.35 mL of dosing solution was added in duplicate to the apical side of the transwell, and transwells transferred into the receiver plate solutions. Transwell plates were then incubated for 1 hour, after which inserts were removed to an empty plate to prevent any further permeation of the compound. 100 µL of solution from donor, receiver wells are removed to a 96 well plate alongside 100 µL of dosing solution. 150 µL of acetonitrile containing internal standard (e.g. 100 ng/mL sulfadimethoxine) is then added to all samples

prior to analysis by LC-MS/MS. Bupropion (positive control) and Atenolol (negative control) were run alongside test compounds. To confirm monolayer integrity, a further 100 µL from each compartment is added to the 96-well F-bottomed microtitre plate containing the Lucifer Yellow standard curve for fluorescence determination of Lucifer Yellow concentrations.

Intrinsic Clearance of Test Compounds in Liver Microsomes. Test compound (0.5 µM) was incubated with female CD1 mouse liver microsomes (Xenotech LLC TM; 0.5 mg/mL 50 mM potassium phosphate buffer, pH 7.4), and the reaction started with the addition of excess NADPH (8 mg/mL 50 mM potassium phosphate buffer, pH 7.4). Immediately, at time zero, then at 3, 6, 9, 15, and 30 minutes an aliquot (50 µL) of the incubation mixture was removed and mixed with acetonitrile (100 µL) to stop the reaction. The internal standard was added to all samples, the samples centrifuged to sediment precipitated protein and the plates were then sealed prior to UPLC-MS/MS analysis.

The rate constant (k) was determined by plotting compound response (the ratio of peak area of test compound to internal standard) at each timepoint and applying an exponential decay equation. The rate of intrinsic clearance (CLi) of each test compound was then calculated using the following calculation: CLi (mL/min/g liver) = k x V x Microsomal protein yield. Microsomal protein yield: 48 mg protein/g liver (mouse) and 39.7 mg protein/g liver (human).

Intrinsic Clearance of Test Compounds in Cryopreserved Hepatocytes. Vials of cryopreserved mouse hepatocytes (Xenotech LLC) and human hepatocytes (Life Technologies) were thawed according to the manufacturer's instructions, and cells were resuspended in Williams Medium E containing cell maintenance supplement pack (CM4000, Life Technologies). Hepatocytes were incubated in suspension (0.5 million cells/mL) in 48 well non-collagen coated cell culture plates for 10 minutes at 37 °C, 5 % CO_2. Upon addition of an equal volume of supplemented Williams Medium E containing 1 µM test compound, an aliquot of incubation solution was removed to 80 µL of acetonitrile containing internal standard (final concentration 0.5 µM test compound and a cell density of 0.25 million cells/mL). Similarly, aliquots were removed at 3, 6, 9, 15, 30, 45, 60, 90, and 120 minutes. 100 µL of 80:20 water:acetonitrile was added to all samples, and the

analysis plate was centrifuged for 10 min at room temperature prior to injection and analysis of samples by UPLC-MS/MS. The response (area ratio of the test compound to internal standard) was plotted against time using an exponential decay model, and the rate of disappearance was calculated. Hepatocyte CLint (mL/min/10^6 cells) was scaled to in vivo CLint (ml/min/g Liver) using the hepatocellularity scaling factor of 135 x 10^6 (mouse) and 118 x 10^6 (human) cells/g of liver.

In vivo pharmacokinetics. Six female mice of the BALB/c strain were obtained from Charles River Laboratories, UK. Animals were maintained under a 12-h light / 12-h dark cycle, in open-top caging containing Chips7D bedding (Datesand Group, UK), with ad libitum access to food (RM1; Special Diet Services, UK) and water. Temperature and relative humidity were maintained between 20-24 °C and 45-65 % respectively. All animals received a minimum of 10 days acclimatization prior to the start of the study.

Dose formulations were prepared on the day of dosing. For the intravenous formulation, the test compound was dissolved in dimethyl sulfoxide (Fisher Bioreagents), then diluted with Polyethylene glycol-400 (Sigma) and 0.9 % w/v saline. The resulting formulation contained 0.2 mg/mL of test compound in a solution of 5 % dimethyl sulfoxide, 40% polyethylene glycol-400 and 55% saline. This formulation was administered via bolus injection at a dose level of 1 mg/kg.

For the oral formulation, the test compound was suspended in 0.5% hydroxypropylmethylcellulose (Methocel K15M Premium USP/EP; Colorcon) in water, at a concentration of 0.3 mg/mL. This formulation was administered by gavage at a dose level of 3 mg/kg. Animals were observed regularly after dose administration.

Serial blood samples (10 µL per sample) were collected from the lateral tail vein prior to dosing for the oral group, then from both groups at 5, 15 and 30 min, 1, 2, 4, 6, 8 and 24 h after the administration of the test compound. Each blood sample was diluted into 90 µL of Milli-Q ultrapure water, and stored at 20 °C prior to bioanalysis by UPLC-MS/MS.

Associated Content:

Additional Data File 1 in csv format: X-ray Data Collection and Protein Structure Refinement Statistics
Molecular Formula Strings File in csv format.

PDB ID Codes:

Atomic coordinates and experimental data have been deposited in the PDB with the following PDB ID codes: MulDHFR:**3** – 8F81; MulDHFR:**4** – 8F84; MulDHFR:**8** – 8TA1; MulDHFR:**9** – 8TBR; MulDHFR:**10** – 8F85; MuLDHFR:**11** – 8F82; MulDHFR:**12** – 8F83; MulDHFR:**14** – 8TA0; MulDHFR:**15** – 8F80.

Corresponding Author Information:

Rafael M. Couñago: rafael.counago@unc.edu
Ronaldo A. Pilli: rapilli@unicamp.br

Present/Current Author Addresses:

M.A.M.: Department of Chemistry, Biochemistry and Pharmaceutical Sciences, University of Bern, Freiestrasse 3, 3012, Bern, Switzerland; I.T.: Libbs Farmacêutica Ltda., Rua Alberto Correia Francfort, 88, Embu das Artes, São Paulo 06807461, Brazil; J.R.S.: Department of Molecular Biology, Center for Computational and Integrative Biology, Massachusetts General Hospital, Boston 02114, Massachusetts, USA; C.V.R.: Department of Biochemistry, University of Cambridge, Sanger Building, 80, Tennis Court Road, CB2 1QW, Cambridge, UK; G.P.R. and V.M.A.: Eurofarma Laboratórios S/A, 06696-000-Itapevi, SP, Brazil; R.M.C.: Structural Genomics Consortium and Division of Chemical Biology and Medicinal Chemistry, UNC Eshelman School of Pharmacy, University of North Carolina, Chapel Hill, North Carolina 27599, USA.

Author Contribution:

# These authors contributed equally to this work.

Conflict of Interest Statement:

All authors declare no competing financial interest.

Acknowledgments

Vasconcelos and Gustavo Riboldi. We thank all members of the Seattle Structural Genomics Center for Infectious Disease (SSGCID) for providing support for the structure determination pipeline including Brad Hammerson, Jan Abendroth and Don Lorimer. We thank all members of the Structure-Guided Drug Discovery Coalition (SDDC) for engaging in discussions and sharing insights and suggestions, including Christopher Walpole and Santha Santhakumar. We thank the staff of the Life Sciences Core Facility (LaCTAD) at UNICAMP for the Genomics and Mass Spectrometry analysis. We thank the NMR facility at UNICAMP Chemistry Institute for its assistance. This research used the Advanced Light Source resources, a DOE Office of Science User Facility under contract no. DE-AC02-05CH11231. The ALS-ENABLE beamlines are supported by the National Institutes of Health, National Institute of General Medical Sciences, grant P30 GM124169-01.

Funding

Abbreviations used:

1,1'-Ferrocenediyl-bis(diphenylphosphine) (dppf); 2,2,6,6-Tetramethylpiperidinyl (TMP); acetic acid (AcOH); acetonitrile (ACN); Advanced Photon Source (APS);

attenuated Total Reflectance (ATR); broad singlet (bs); calculated (calc.); Deuterochloroform (CD); dichloromethane (DCM); dimethylformamide (DMF); dihydrofolate reductase (DHFR); dimethyl sulfoxide (DMSO); doublet (d); ethanol (EtOH); electrospray ionization mass spectrometry (ESI); equivalent (equiv.); formic acid (FA); half-maximal inhibitory concentrations (IC_{50}); Hertz (Hz); high-performance liquid chromatography (HPLC); high-resolution mass spectra (HRMS); human DHFR (HsaDHFR); human liver microsomes (HLM); infrared (IF); inhibitory constant (K_i); intrinsic clearance (CLi); isopropyl 1-thio-D-galactopyranoside (IPTG); liquid chromatography mass spectrometry (LC-MS); Madin-Darby canine kidney (MDCK); multiplet (m); nicotinamide adenine dinucleotide phosphate (NADPH); nuclear magnetic resonance (NMR); nucleophilic aromatic substitution (SNAr); minimum inhibitory concentration (MIC); *Mycobacteria abscessus* DHFR (MabDHFR), *Mycobacteria avium* DHFR (MavDHFR); part per million (ppm); quartet (q); quintet (quint); resazurin microtiter assay (REMA); room temperature (r.t.); saturated aqueous (sat. aq.); singlet (s); sodium hydride (NaH); tetrahydrofuran (THF); thin layer chromatography (TLC); time-of-flight mass spectrometry (TOF); trans,trans-dibenzylidene acetone (dba); trifluoroacetic acid (TFA); triethylamine (Et$_3$N); triplet (t).

References

1. Falkinham, I., J. O. Surrounded by mycobacteria: nontuberculous mycobacteria in the human environment. *Journal of Applied Microbiology* **107**, 356–367 (2009).

2. Baldwin, S. L., Larsen, S. E., Ordway, D., Cassell, G. & Coler, R. N. The complexities and challenges of preventing and treating nontuberculous mycobacterial diseases. *PLoS Negl Trop Dis* **13**, e0007083 (2019).

3. Prato, B. D. *et al.* Non-tuberculous Mycobacterial Pulmonary Disease: an Italian National Survey. *Sarcoidosis Vasc Diffuse Lung Dis* **35**, 21–25 (2018).

4. Shah, N. M. *et al.* Pulmonary Mycobacterium avium-intracellulare is the main driver of the rise in non-tuberculous mycobacteria incidence in England, Wales and Northern Ireland, 2007–2012. *BMC Infectious Diseases* **16**, 195 (2016).

5. Yu, X. *et al.* Identification and Characterization of Non-Tuberculous Mycobacteria Isolated from Tuberculosis Suspects in Southern-Central China. *PLOS ONE* **9**, e114353 (2014).

6. Marras, T. K., Chedore, P., Ying, A. M. & Jamieson, F. Isolation prevalence of pulmonary non-tuberculous mycobacteria in Ontario, 1997–2003. *Thorax* **62**, 661–666 (2007).

7. Moore, J. E., Kruijshaar, M. E., Ormerod, L. P., Drobniewski, F. & Abubakar, I. Increasing reports of non-tuberculous mycobacteria in England, Wales and Northern Ireland, 1995-2006. *BMC Public Health* **10**, 612 (2010).

8. Jain, S., Sankar, M. M., Sharma, N., Singh, S. & Chugh, T. D. High prevalence of non-tuberculous mycobacterial disease among non-HIV infected individuals in

a TB endemic country – experience from a tertiary center in Delhi, India. *Pathogens and Global Health* **108**, 118–122 (2014).

9. Lai, C.-C. *et al.* Increasing Incidence of Nontuberculous Mycobacteria, Taiwan, 2000–2008. *Emerg. Infect. Dis.* **16**, 294–296 (2010).

10. Adjemian, J., Olivier, K. N., Seitz, A. E., Holland, S. M. & Prevots, D. R. Prevalence of Nontuberculous Mycobacterial Lung Disease in U.S. Medicare Beneficiaries. *Am J Respir Crit Care Med* **185**, 881–886 (2012).

11. Daley, C. L. *et al.* Treatment of nontuberculous mycobacterial pulmonary disease: an official ATS/ERS/ESCMID/IDSA clinical practice guideline. *Eur Respir J* **56**, 2000535 (2020).

12. Saxena, S., Spaink, H. P. & Forn-Cuní, G. Drug Resistance in Nontuberculous Mycobacteria: Mechanisms and Models. *Biology* **10**, 96 (2021).

13. Sim, Y. S. *et al.* Standardized Combination Antibiotic Treatment of *Mycobacterium avium* Complex Lung Disease. *Yonsei Med J* **51**, 888 (2010).

14. Wallace, R. J. *et al.* Clinical experience in 52 patients with tigecycline-containing regimens for salvage treatment of Mycobacterium abscessus and Mycobacterium chelonae infections. *Journal of Antimicrobial Chemotherapy* **69**, 1945–1953 (2014).

15. Diagnosis and Treatment of Disease Caused by Nontuberculous Mycobacteria. *Am J Respir Crit Care Med* **156**, S1–S25 (1997).

16. Wu, M.-L., Aziz, D. B., Dartois, V. & Dick, T. NTM drug discovery: status, gaps and the way forward. *Drug Discovery Today* **23**, 1502–1519 (2018).

17. Van Ingen, J., Hoefsloot, W., Dartois, V. & Dick, T. Rifampicin has no role in treatment of *Mycobacterium avium* complex pulmonary disease and

bactericidal sterilising drugs are needed: a viewpoint. *Eur Respir J* **63**, 2302210 (2024).

18. Mirsaeidi, M., Farshidpour, M., Allen, M. B., Ebrahimi, G. & Falkinham, J. O. Highlight on Advances in Nontuberculous Mycobacterial Disease in North America. *BioMed Research International* **2014**, 1–10 (2014).

19. Conyers, L. E. & Saunders, B. M. Treatment for non-tuberculous mycobacteria: challenges and prospects. *Front. Microbiol.* **15**, 1394220 (2024).

20. Kohanski, M. A., Dwyer, D. J. & Collins, J. J. How antibiotics kill bacteria: from targets to networks. *Nat Rev Microbiol* **8**, 423–435 (2010).

21. Wróbel, A., Arciszewska, K., Maliszewski, D. & Drozdowska, D. Trimethoprim and other nonclassical antifolates an excellent template for searching modifications of dihydrofolate reductase enzyme inhibitors. *J Antibiot* **73**, 5–27 (2020).

22. Zhao, F. *et al.* Binding Pocket Alterations in Dihydrofolate Synthase Confer Resistance to *para* -Aminosalicylic Acid in Clinical Isolates of Mycobacterium tuberculosis. *Antimicrob Agents Chemother* **58**, 1479–1487 (2014).

23. Zheng, J. *et al.* para-Aminosalicylic Acid Is a Prodrug Targeting Dihydrofolate Reductase in Mycobacterium tuberculosis. *Journal of Biological Chemistry* **288**, 23447–23456 (2013).

24. Nixon, M. R. *et al.* Folate Pathway Disruption Leads to Critical Disruption of Methionine Derivatives in Mycobacterium tuberculosis. *Chemistry & Biology* **21**, 819–830 (2014).

25. Rosowsky, A., Forsch, R. A. & Queener, S. F. Inhibition of *Pneumocystis carinii* , *Toxoplasma gondii* , and *Mycobacterium avium* Dihydrofolate Reductases by

2,4-Diamino-5-[2-methoxy-5-(ω-carboxyalkyloxy)benzyl]pyrimidines: Marked Improvement in Potency Relative to Trimethoprim and Species Selectivity Relative to Piritrexim. *J. Med. Chem.* **45,** 233–241 (2002).

26. Rosowsky, A., Forsch, R. A. & Queener, S. F. Further Studies on 2,4-Diamino-5-(2',5'-disubstituted benzyl)pyrimidines as Potent and Selective Inhibitors of Dihydrofolate Reductases from Three Major Opportunistic Pathogens of AIDS. *J. Med. Chem.* **46**, 1726–1736 (2003).

27. Forsch, R. A., Queener, S. F. & Rosowsky, A. Preliminary in vitro studies on two potent, water-soluble trimethoprim analogues with exceptional species selectivity against dihydrofolate reductase from Pneumocystis carinii and Mycobacterium avium. *Bioorganic & Medicinal Chemistry Letters* **14**, 1811–1815 (2004).

28. Rosowsky, A., Fu, H., Chan, D. C. M. & Queener, S. F. Synthesis of 2,4-Diamino-6-[2'- *O* -(ω-carboxyalkyl)oxydibenz[*b* , *f*]azepin-5-yl]methylpteridines as Potent and Selective Inhibitors of *Pneumocystis c arinii, Toxoplasma g ondii* , and *Mycobacterium a vium* Dihydrofolate Reductase. *J. Med. Chem.* **47**, 2475–2485 (2004).

29. Rosowsky, A., Forsch, R. A., Sibley, C. H., Inderlied, C. B. & Queener, S. F. New 2,4-Diamino-5-(2',5'-substituted benzyl)pyrimidines as Potential Drugs against Opportunistic Infections of AIDS and Other Immune Disorders. Synthesis and Species-Dependent Antifolate Activity. *J. Med. Chem.* **47**, 1475–1486 (2004).

30. Chan, D. C. M., Fu, H., Forsch, R. A., Queener, S. F. & Rosowsky, A. Design, Synthesis, and Antifolate Activity of New Analogues of Piritrexim and Other Diaminopyrimidine Dihydrofolate Reductase Inhibitors with ω-Carboxyalkoxy

or ω-Carboxy-1-alkynyl Substitution in the Side Chain. *J. Med. Chem.* **48**, 4420–4431 (2005).

31. Aragaw, W. W. *et al.* Pharmacological validation of dihydrofolate reductase as a drug target in *Mycobacterium abscessus*. *Antimicrob Agents Chemother* **68**, e00717-23 (2024).

32. Ribeiro, J. A. *et al.* Using a Fragment-Based Approach to Identify Alternative Chemical Scaffolds Targeting Dihydrofolate Reductase from *Mycobacterium tuberculosis*. *ACS Infect. Dis.* **6**, 2192–2201 (2020).

33. Yuthavong, Y. *et al.* Malarial dihydrofolate reductase as a paradigm for drug development against a resistance-compromised target. *Proc. Natl. Acad. Sci. U.S.A.* **109**, 16823–16828 (2012).

34. Riboldi, G. P. *et al.* Identification of P218 as a potent inhibitor of *Mycobacterium ulcerans* DHFR. *RSC Med. Chem.* **12**, 103–109 (2021).

35. Chughlay, M. F. *et al.* Chemoprotective Antimalarial Activity of P218 against Plasmodium falciparum: A Randomized, Placebo-Controlled Volunteer Infection Study. *The American Journal of Tropical Medicine and Hygiene* **104**, 1348–1358 (2021).

36. Kreutzfeld, O. *et al.* Decreased Susceptibility to Dihydrofolate Reductase Inhibitors Associated With Genetic Polymorphisms in Ugandan *Plasmodium falciparum* Isolates. *The Journal of Infectious Diseases* **225**, 696–704 (2022).

37. Pethrak, C. *et al.* New Insights into Antimalarial Chemopreventive Activity of Antifolates. *Antimicrob Agents Chemother* **66**, e01538-21 (2022).

38. Luthra, S., Rominski, A. & Sander, P. The Role of Antibiotic-Target-Modifying and Antibiotic-Modifying Enzymes in Mycobacterium abscessus Drug Resistance. *Front. Microbiol.* **9**, 2179 (2018).

39. Van Ingen, J., Boeree, M. J., Van Soolingen, D. & Mouton, J. W. Resistance mechanisms and drug susceptibility testing of nontuberculous mycobacteria. *Drug Resistance Updates* **15**, 149–161 (2012).

40. Lambert, R. J. W. & Pearson, J. Susceptibility testing: accurate and reproducible minimum inhibitory concentration (MIC) and non-inhibitory concentration (NIC) values. *J Appl Microbiol* **88**, 784–790 (2000).

41. Li, R. *et al.* Three-dimensional structure of M. tuberculosis dihydrofolate reductase reveals opportunities for the design of novel tuberculosis drugs. *Journal of Molecular Biology* **295**, 307–323 (2000).

42. Dwane, L. *et al.* Project Score database: a resource for investigating cancer cell dependencies and prioritizing therapeutic targets. *Nucleic Acids Research* **49**, D1365–D1372 (2021).

43. Ahmadzadeh, A., Zamani, N., Hassanian-Moghaddam, H., Hadeiy, S. K. & Parhizgar, P. Acute versus chronic methotrexate poisoning; a cross-sectional study. *BMC Pharmacol Toxicol* **20**, 39 (2019).

44. Meirelles, M. A. *et al.* Functionalization of 2,4-Dichloropyrimidines by 2,2,6,6-Tetramethylpiperidyl Zinc Base Enables Modular Synthesis of Antimalarial Diaminopyrimidine P218 and Analogues. *J. Org. Chem.* **88**, 9475–9487 (2023).

45. Raaijmakers, J., Schildkraut, J. A., Hoefsloot, W. & Van Ingen, J. The role of amikacin in the treatment of nontuberculous mycobacterial disease. *Expert Opinion on Pharmacotherapy* **22**, 1961–1974 (2021).

46. Gygli, S. M., Borrell, S., Trauner, A. & Gagneux, S. Antimicrobial resistance in Mycobacterium tuberculosis: mechanistic and evolutionary perspectives. *FEMS Microbiology Reviews* **41**, 354–373 (2017).

47. Fanti, R. C. *et al.* A Target Engagement Assay to Assess Uptake, Potency, and Retention of Antibiotics in Living Bacteria. *ACS Infect. Dis.* **8**, 1449–1467 (2022).

48. Richter, M. F. & Hergenrother, P. J. The challenge of converting Gram-positive-only compounds into broad-spectrum antibiotics. *Annals of the New York Academy of Sciences* **1435**, 18–38 (2019).

49. Katsuno, K. *et al.* Hit and lead criteria in drug discovery for infectious diseases of the developing world. *Nat Rev Drug Discov* **14**, 751–758 (2015).

50. Lakshminarayana, S. B. *et al.* Comprehensive physicochemical, pharmacokinetic and activity profiling of anti-TB agents. *Journal of Antimicrobial Chemotherapy* **70**, 857–867 (2015).

51. Myler, P. *et al.* The Seattle Structural Genomics Center for Infectious Disease (SSGCID). *IDDT* **9**, 493–506 (2009).

52. Stacy, R. *et al.* Structural genomics of infectious disease drug targets: the SSGCID. *Acta Crystallogr F Struct Biol Cryst Commun* **67**, 979–984 (2011).

53. Choi, R. *et al.* Immobilized metal-affinity chromatography protein-recovery screening is predictive of crystallographic structure success. *Acta Crystallogr F Struct Biol Cryst Commun* **67**, 998–1005 (2011).

54. Serbzhinskiy, D. A. *et al.* Structure of an ADP-ribosylation factor, ARF1, from *Entamoeba histolytica* bound to Mg $^{2+}$ –GDP. *Acta Crystallogr F Struct Biol Commun* **71**, 594–599 (2015).

55. Bryan, C. M. *et al*. High-throughput protein production and purification at the Seattle Structural Genomics Center for Infectious Disease. *Acta Crystallogr F Struct Biol Cryst Commun* **67**, 1010–1014 (2011).

56. Studier, F. W. Protein production by auto-induction in high-density shaking cultures. *Protein Expression and Purification* **41**, 207–234 (2005).

57. Vedadi, M. *et al*. Genome-scale protein expression and structural biology of Plasmodium falciparum and related Apicomplexan organisms. *Molecular and Biochemical Parasitology* **151**, 100–110 (2007).

58. Gorrec, F. The MORPHEUS protein crystallization screen. *J Appl Crystallogr* **42**, 1035–1042 (2009).

59. Pereira, J. H., McAndrew, R. P., Tomaleri, G. P. & Adams, P. D. Berkeley Screen: a set of 96 solutions for general macromolecular crystallization. *J Appl Crystallogr* **50**, 1352–1358 (2017).

60. Kabsch, W. *XDS*. *Acta Crystallogr D Biol Crystallogr* **66**, 125–132 (2010).

61. Vagin, A. & Teplyakov, A. *MOLREP* : an Automated Program for Molecular Replacement. *J Appl Crystallogr* **30**, 1022–1025 (1997).

62. Winn, M. D. *et al*. Overview of the *CCP* 4 suite and current developments. *Acta Crystallogr D Biol Crystallogr* **67**, 235–242 (2011).

63. Emsley, P., Lohkamp, B., Scott, W. G. & Cowtan, K. Features and development of *Coot*. *Acta Crystallogr D Biol Crystallogr* **66**, 486–501 (2010).

64. Adams, P. D. *et al*. *PHENIX* : a comprehensive Python-based system for macromolecular structure solution. *Acta Crystallogr D Biol Crystallogr* **66**, 213–221 (2010).

65. Chen, V. B. *et al. MolProbity* : all-atom structure validation for macromolecular crystallography. *Acta Crystallogr D Biol Crystallogr* **66**, 12–21 (2010).

66. Savitsky, P. *et al.* High-throughput production of human proteins for crystallization: The SGC experience. *Journal of Structural Biology* **172**, 3–13 (2010).